# Supplementary Material for "Rational design of nanoscale stabilized oxide catalysts for OER with OC22"

Richard Tran,[†] Liqiang Huang,[†] Yuan Zi,[¶] Shengguang Wang,[‡] Benjamin M. Comer,[§] Xuqing Wu,[‖] Stefan J. Raaijman,[§] Nishant K. Sinha,[§] Sajanikumari Sadasivan,[⊥] Shibin Thundiyil,[§] Kuldeep B. Mamtani,[⊥] Ganesh Iyer,[§] Lars Grabow,[‡] Ligang Lu,[§] and Jiefu Chen[¶]

†*Indicates equal contributions*

‡*Department of Chemical and Biomolecular Engineering, University of Houston, 4226 Martin Luther King Boulevard, Houston, TX 77204, USA.*

¶*Department of Electrical and Computer Engineering, University of Houston, 4226 Martin Luther King Boulevard, Houston, TX 77204, USA.*

§*Shell Global Solutions, Houston, TX 77082, USA.*

‖*Department of Information Science Technology, University of Houston, 14004 University Boulevard #318, Sugar Land, TX 77479, USA.*

⊥*Shell Technical Center Bangalore, 7, Bengaluru Hardware Park KIADB Industrial Park North, Mahadeva Kodigehalli, Bengaluru, Bangalore, Karnataka 562149, India.*

E-mail:

## Surface energy

To the surface energy of all bare slabs, we begin with the surface grand potential given by:

$$\gamma = \frac{E_{slab} - \sum_i n_i \mu_i}{2A} \tag{1}$$

where $E_{slab}$ is the total energy of the bare slab, $n_i$ is the number of atom $i$ in the slab, $\mu_i$ is the chemical potential of atom $i$, $A$ is the surface area and the factor of $\frac{1}{2}$ accounts for the two surfaces in the slab. We can define the chemical potential of each element as:

$$\mu_{\mathrm{A_xB_yO_z}} = E_{bulk}^{\mathrm{A_xB_yO_z}} = x\mu_A + y\mu_B + z\mu_O \tag{2}$$

where $E_{bulk}^{\mathrm{A_xB_yO_z}}$ is the total energy per formula unit of the bulk crystal. As such, the surface energy for stoichiometric slabs can be rewritten as:

$$\gamma = \frac{E_{slab}^{\mathrm{A_{nx}B_{ny}O_{nz}}} - nE_{bulk}^{\mathrm{A_xB_yO_z}}}{2A} \tag{3}$$

where n is the number of bulk formula units in the slab.

We reiterate that we enumerated through all terminations per facet by modelling slabs with symmetrically equivalent terminations on each side. Inevitably, this will require the removal or addition of cations and oxygen which will lead to non-stoichiometric (relative to the bulk) slab models. In such cases, we need to compensate for the excess or deficient components by introducing variable chemical potentials per component. For any slab, there can be up to $n-1$ excess or deficient components relative to the bulk. As an example, the surface energy of a slab of $\mathrm{A_{nx}B_{ny+k}O_{nz\text{-}j}}$ constructed from a bulk crystal of $\mathrm{A_xB_yO_z}$ becomes:

$$\gamma = \frac{E_{slab}^{\mathrm{A_{nx}B_{ny+k}O_{nz-j}}} - (nE_{bulk}^{\mathrm{A_xB_yO_z}} + k\mu_B - j\frac{1}{2}\mu_{O_2})}{2A} \tag{4}$$

The chemical potential of oxygen ($\mu_O$) can be referenced to the electrochemical decom-

position of water to $O_{2(g)}$:

$$2H_2O_{(g)} \rightarrow 4(H^+ + e^-) + O_{2(g)} : \qquad 4.92\ eV \tag{5}$$

given by:

$$\mu_{O_2} = 4.92 + 2G_{H_2O} - 4(\mu_{H^+} + \mu_{e^-}) + \Delta G^{O^*}_{corr} \tag{6}$$

where

$$G = E + ZPE - TS^o \tag{7}$$

We can relate the proton-electron pair $(H^+ + e^-)$ to the activity of the proton and the standard hydrogen electrode (SHE) using the Nernst Equation:

$$\mu_{H^+} + \mu_{e^-} = \frac{1}{2}G_{H_2} - eU + k_B T ln a_{H^+} \tag{8}$$

Here $a_{H^+}$ is the activity of a proton with $-pHln10 = lna_{H^+}$ and $eU$ is the change in electron energy under an applied potential. An excess or deficient oxygen component in the slab can be treated as an adsorbed or desorbed species and to account for this, we included a correction term, $\Delta G^{O^*}_{corr}$, to derive the Gibbs free energy of adsorption from the Density Functional Theory (DFT) electronic O* adsorption energy (see Tran et al.[1] and Gunasooriya and Nørskov[2] for details in regards to corrections made for the Gibbs free energy). Consequently, $\mu_O$ can be rewritten as a function of $pH$ and $U$ as such:

$$\mu_{O_2} = 4.92 + 2\mu_{H_2O} - 4(\frac{1}{2}\mu_{H_2} - eU + k_B T ln a_{H^+}) + \Delta G^{O^*}_{corr} \tag{9}$$

It is typical to reference the chemical potential of B ($\mu_B$) with respect to the per atom energy of the ground state bulk crystal of pure component B (e.g. $\mu_{Fe} = \Delta\mu_{Fe} + E^{DFT}_{BCC,Fe}$). However, this is predicated upon the assumption that $A_xFe_yO_z$ will immediately decompose into pure solid BCC Fe at the surface. However, multicomponent systems generally do not

immediately decompose into individual solid components of each element. Herein, we assume that an excess or deficiency of components B or O at the surface will lead to slight surface passivation with a decomposition of $A_xB_yO_z$ into a more stable multicomponent guided by the phase diagram, e.g.:

$$A_xB_yO_z \rightarrow xA + B_yO_z \tag{10}$$

In such a case, it makes sense to reference $\mu_B$ with respect to the energy of $B_yO_z$:

$$\mu_{B_yO_z} = E_{bulk}^{B_yO_z} = y\mu_B + z\mu_O \tag{11}$$

Here, the chemical potential of B increases (or decreases) with the component of B at the surface, leading to a slight passivation of $A_xB_yO_z$ to $B_yO_z$ at the surface. We can thereby rewrite $\mu_B$ as a function of $\mu_O$

$$\mu_B = \frac{E_{bulk}^{B_yO_z} - z\mu_O}{y} \tag{12}$$

which can be substituted into Equation 4 in order to define surface energy purely as a function of $\mu_O$ and by extension $U$ and $pH$ in accordance with Equation 9.

## Nanoparticle formation energy

The nanoparticle formation energy ($G_f^{NP}$) is given by Equation 4 in the main manuscript. For a material in the bulk regime ($r > 100$ nm), we can assume that the thermodynamic contributions of the surface are negligible when compared to the contribution from the bulk. However, as the particle size continues to decrease, the surface-area-to-volume ratio will increase, resulting the properties of the surface dictating the properties of the overall material. Unlike the bulk formation energy ($E_V(pH, V, T)(\frac{4}{3}\pi r^3)$), $G_f^{NP}$ accounts for this by incorporating the surface energy contributions into the overall formation energy.

Here, $\frac{4}{3}\pi r^3$ is the volume of a nanoparticle at radius $r$ and $E_V$ is the Pourbaix formation energy at a given pH, U, and T per unit cell volume ($E_{PBX}/V$) where $E_{PBX}$ can be derived

from the following:[3–5]

$$E_{PBX} = E_0 + k_B T ln(10) pH - n_O \mu^o_{\mathrm{H_2O}} + (n_H - 2n_O) pH + n_{e^-}(-n_H + 2n_O + eU) \quad (13)$$

where $n$ are the number of species in the system respectively and $E_0$ is the formation energy of the bulk with respect to $\mathrm{H}_{2(g)}$ and $\mathrm{O}_{2(g)}$:

$$E_0 = E_f + k_B T ln(10) pH - n_{\mathrm{H_2O}} \mu^o_{\mathrm{H_2O}} \quad (14)$$

The contribution of the surface energy is given by $\bar{\gamma}(4\pi r^2)$ where $4\pi r^2$ is the surface area of the nanoparticle at radius $r$ and $\bar{\gamma}$ is the surface energy of the nanoparticle. In this study, the equilibrium crystal structure, or Wulff shape, serves as an analogue to the nanoparticle. The Wulff shape is derived through the Wulff construction whereby a set of Miller index (hkl) planes perpendicular to a vector from an origin at a distance proportional to $\gamma_{hkl}$ (see Equation 1 in the main manuscript) enclose a polyhedron. The surface energy of this polyhedron is defined by:

$$\bar{\gamma}(pH, U, T, \Delta\mu_M) = \frac{\sum_{hkl} \gamma_{hkl}(pH, U, T, \Delta\mu_M) A_{hkl}}{\sum_{hkl} A_{hkl}} = \sum_{hkl} \gamma_{hkl} f^A_{hkl}(pH, U, T, \Delta\mu_M) \quad (15)$$

where $(hkl)$ are the facets that appear on the Wulff shape and $f^A_{hkl}$ is the fraction of area occupied by facet $(hkl)$ on the Wulff shape.

Incorporating the surface energy contributions of the nanoparticle can consequently lead to some materials above the Pourbaix hull becoming more thermodynamically stable than the ground state material depending on the nanoparticle size.

## Overpotential

The overpotential has been demonstrated to be an excellent predictor of catalytic activity in electrocatalytic processes. The overpotential ($\eta$) describes the excess amount of applied

potential required to move forward in each reaction step shown in Figure 3 relative to an ideal catalyst. The summation of each reaction energy (energetic height of each reaction step or $\Delta G_{rxn}$) is defined as the standard reduction potential in Equation 5. The ideal catalyst equally distributes the standard reduction potential along each step to minimize the required energy needed to move the reaction in the forward direction. This required energy is the equilibrium potential of oxygen evolution reaction (OER) and is given as:

$$\frac{G_{\mathrm{O_2}} + 2G_{\mathrm{H_2}} - 2G_{\mathrm{H_2O}}}{4e}/ = 1.23V \tag{16}$$

As such, the theoretical overpotential for an electrocatalyst is given by:

$$\eta^{OER} = max(\Delta G^1_{rxn}, \Delta G^2_{rxn}, \Delta G^3_{rxn}, \Delta G^4_{rxn})/e - 1.23V \tag{17}$$

where $max(\Delta G^1_{rxn}, \Delta G^2_{rxn}, \Delta G^3_{rxn}, \Delta G^4_{rxn})$ is the reaction energy of the potential determining step or $\Delta G^{RDS}_{rxn}$.

The energy of each reaction step is relative to the energy of a bare slab and two water molecules in a vacuum, all of which are initially assumed to be non-interacting. Guided by Equations i-iv (see Figure 3, we can determine the DFT electronic adsorption energy of steps i-iii with the following:

$$E^{\mathrm{OH}^*}_{ads} = E^{\mathrm{OH}^*} + \frac{1}{2}E_{\mathrm{H_2}} - E_{slab} - \mu^o_{\mathrm{H_2O}} \tag{18}$$

$$E^{\mathrm{O}^*}_{ads} = E^{\mathrm{O}^*} + E_{\mathrm{H_2}} - E_{slab} - \mu^o_{\mathrm{H_2O}} \tag{19}$$

$$E^{\mathrm{OOH}^*}_{ads} = E^{\mathrm{OOH}^*} + \frac{3}{2}E_{\mathrm{H_2}} - E_{slab} - 2\mu^o_{\mathrm{H_2O}} \tag{20}$$

where $E^{X^*}$ is the total energy of the surface intermediate with adsorbate $X$ and $E_X$ is the reference energy of the adsorbate in a gas. By incorporating the vibrational frequency contributions of the adsorbate on the surface in $E^{ads*}$, i.e. the zero point energy and entropy,

we can derive the corresponding Gibbs adsorption energies for steps i-iv:

$$\Delta G^{i} = G^{\mathrm{OH}^*} + \mu_{H^+} + \mu_{e^-} - E_{slab} - G_{\mathrm{H_2O}} \tag{21}$$

$$\Delta G^{ii} = G^{\mathrm{O}^*} + 2(\mu_{H^+} + \mu_{e^-}) - E_{slab} - G_{\mathrm{H_2O}} \tag{22}$$

$$\Delta G^{iii} = G^{\mathrm{OOH}^*} + 3(\mu_{H^+} + \mu_{e^-}) - E_{slab} - 2G_{\mathrm{H_2O}} \tag{23}$$

$$\Delta G^{iv} = 4.92V = G_{\mathrm{O_2}} + 4(\mu_{H^+} + \mu_{e^-}) - 2G_{\mathrm{H_2O}} \tag{24}$$

As previously mentioned, a constant correction term ($\Delta G_{corr}$) can also be added to Equations 18-20 to obtain $\Delta G$:

$$\Delta G^{i} = E_{ads}^{\mathrm{OH}^*} + \Delta G_{corr}^{OH^*} + \mu_{H^+} + \mu_{e^-} \tag{25}$$

$$\Delta G^{ii} = E^{\mathrm{O}^*} + \Delta G_{corr}^{OH^*} + 2(\mu_{H^+} + \mu_{e^-}) \tag{26}$$

$$\Delta G^{iii} = E^{\mathrm{OOH}^*} + \Delta G_{corr}^{OH^*} + 3(\mu_{H^+} + \mu_{e^-}) \tag{27}$$

where $G_{corr}^{OH^*}$, $G_{corr}^{O^*}$, and $G_{corr}^{OOH^*}$ were derived in the Supplementary Information of Open Catalyst 2022 (OC22).[1] Alternatively, if $E^{OOH^*}$ is unavailable, well known scaling relationships between $\Delta G^{iii}$ and $\Delta G^{i}$ can be used instead (Figure S1)):

$$\Delta G^{iii} = \Delta G^{i} + 3.26 \tag{28}$$

From Equations 21-24 we can then obtain the individual reaction energies list in Figure 1:

$$\Delta G_{rxn}^{1} = G^{i} \tag{29}$$

$$\Delta G_{rxn}^{2} = G^{ii} - G^{i} \tag{30}$$

$$\Delta G_{rxn}^{3} = G^{iii} - G^{ii} \tag{31}$$

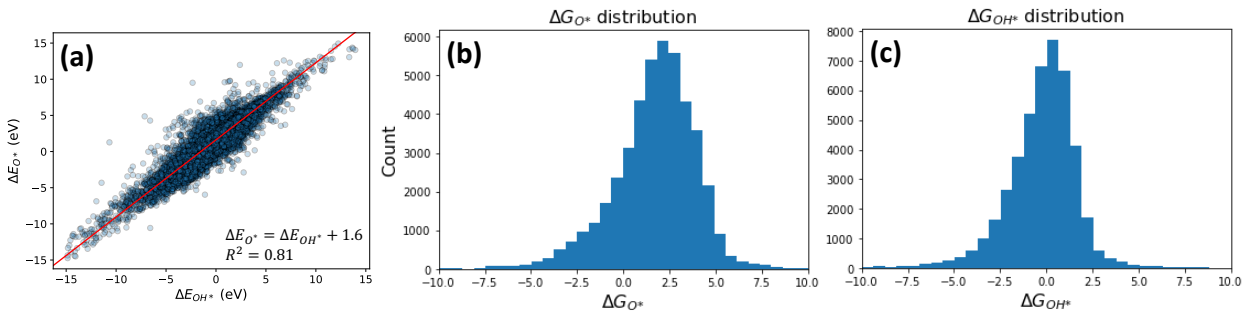


Figure 1: (a) Scaling relationship between $\Delta G_{OH^*}$ and $\Delta G_{O^*}$. Binding energies of $\Delta G > 15eV$ or $\Delta G < -15eV$ were omitted from scaling relationship as anomalies. Distribution of adsorption energies for $\Delta G_{O^*}$ (b) and $\Delta G_{OH^*}$ (c).

$$\Delta G^4_{rxn} = 4.92 - G^{iii} \tag{32}$$

## Predictions of OOH* and dissociation and desorption events

To save computational resources and time, we performed all initial assessments of $\eta$ for all surfaces by predicting the Gibbs free energy of OH* and O* with Machine learning (ML) and OOH* using the scaling relationship provided by Equation 28. We acknowledge that this is a key intermediate in the water nucleophilic attack (WNA) mechanism and by avoiding this step, it is unclear if candidate catalysts will undergo alternative mechanisms for OER. Furthermore, Equation 28 confines our exploration of overpotentials to the theoretical limit of 0.3-0.37 V regardless if any candidate studied can potentially break scaling relationships. Subsequently, we predicted the OOH* intermediate for all surfaces exhibiting $\eta < 0.75V$. Figure S2(a) shows the OOH* Gibbs free energy ($\Delta G^{iii}$) of adsorption of these surfaces using Equation 28 (x-axis) and ML predicted $E_{ads}^{\mathrm{OOH}^*}$. Although a large majority of data points lie within a mean absolute error (MAE) of 0.4 eV (62% or 5,861 out of 9,516 datapoints), we find that most data points beyond the MAE illustrates the predicted $\Delta G^{iii}$ will severely underestimate the corresponding value obtained through a scaling relationship. We also find that the majority of overpotential data points (65% or 2,324 out of 3,554 data points) assessed using both methods will consistently fall below 0.75 V, albeit with 2,368 within the MAE.

In predicting the overpotential of each surface, we also initially applied a spring constant of $7.5eV/\mathring{A}^{-2}$ between all adsorbate atoms and $2eV/\mathring{A}^{-2}$ between the surface and adsorbate to avoid desorption and dissociation events. However, this could lead to final geometries far away from the energy minima, resulting in poor energy predictions and unreliable geometries. Subsequently, for all predictions of intermediates that contributed to a free energy diagram exhibiting $\eta < 0.75V$, we performed additional ML relaxation steps on the final predicted geometries (obtained with constraints induced by the spring constant) *sans* the constraints. This two step relaxation process will help minimize the number of dissociation and desorption events when possible while providing the most reliable predicted geometries. Figure S2(c) plots the Gibbs free energy of the three intermediates obtained with constraints (x-axis) and without constraints (y-axis). We find the intermediates relaxing to a lower energy minima once the constraints were lifted. A large number of data points considered exhibit dissociation and/or desorption when the constraints were lifted resulting in a large MAE of 0.38 eV. A vast majority of these datapoints correspond to the OOH* intermediate. However, the Gibbs free energy of adsorption for dissociated or desorbed intermediates can not be appropriately interpreted due to the lack of adsorption. As such, we also evaluated the MAE for intermediates where these events did not occur in both methods of predictions and demonstrated a more reasonable MAE of 0.17 eV. Figure S2(d) shows the corresponding overpotentials interpreted from these two sets of Gibbs free energy and shows a similar behavior in MAE when dissocition and desorption events are considered or omitted. Figure S2(e) shows a barplot distribution of the absolute difference in overpotential when considering the two methods of prediction. Although a significant amount of data points do exhibit dissociation and desorption with some overpotentials having inconsistent rate determining steps across the two methods, we see that these data points most correspond to larger disparities in overpotential with the majority of data points have a disparity of less than 0.25.

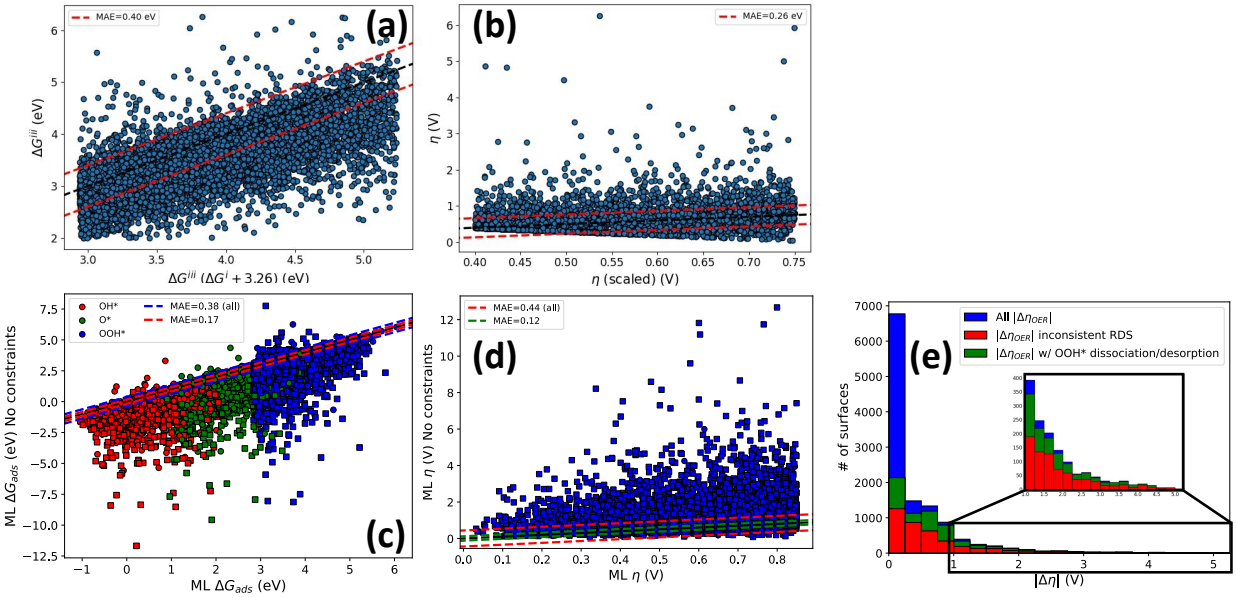


Figure 2: (a) Comparison of Gibbs free energy of adsorption for OOH* ($\Delta G^{iii}$) using Equation 28 (x-axis) vs $\Delta G^{iii}$ using Equation 23 with ML predictions of $E_{ads}^{\mathrm{OOH}^*}$ (b) and the corresponding data points for overpotential. (c) Comparison of the Gibbs free energy of adsorption ($\Delta G_{ads}$) with spring constraints to prevent adsorbate dissociation and desorption (x-axis) and without (y-axis) (d) and the corresponding data points for overpotential. Square data points indicate dissociation or desorption. The blue dashed line corresponds to an MAE when all data points are considered and the red dashed line indicates an MAE with dissociation and desorption events ommitted. (e) Distribution in the absolute difference in overpotential between values calculated with and without the aforementioned constraints with an inset for datapoints exhibit a difference greater than 1.0 V.

## Database usage

The entire database including the initial and relaxed structures and total energies are freely available through the University of Houston Dataverse Repository.[6] The database comes in 4,119 .json files (one for each material assessed) with the mpid name followed by the '.json' suffix (e.g. mp-775737.json). Each file contains a list of dictionary objects. Each dictionary contains the metadata and predicted information of a specific surface and all the surface intermediates (O*, OH*, and OOH*) of that surface and is structured as shown in Figure S3:

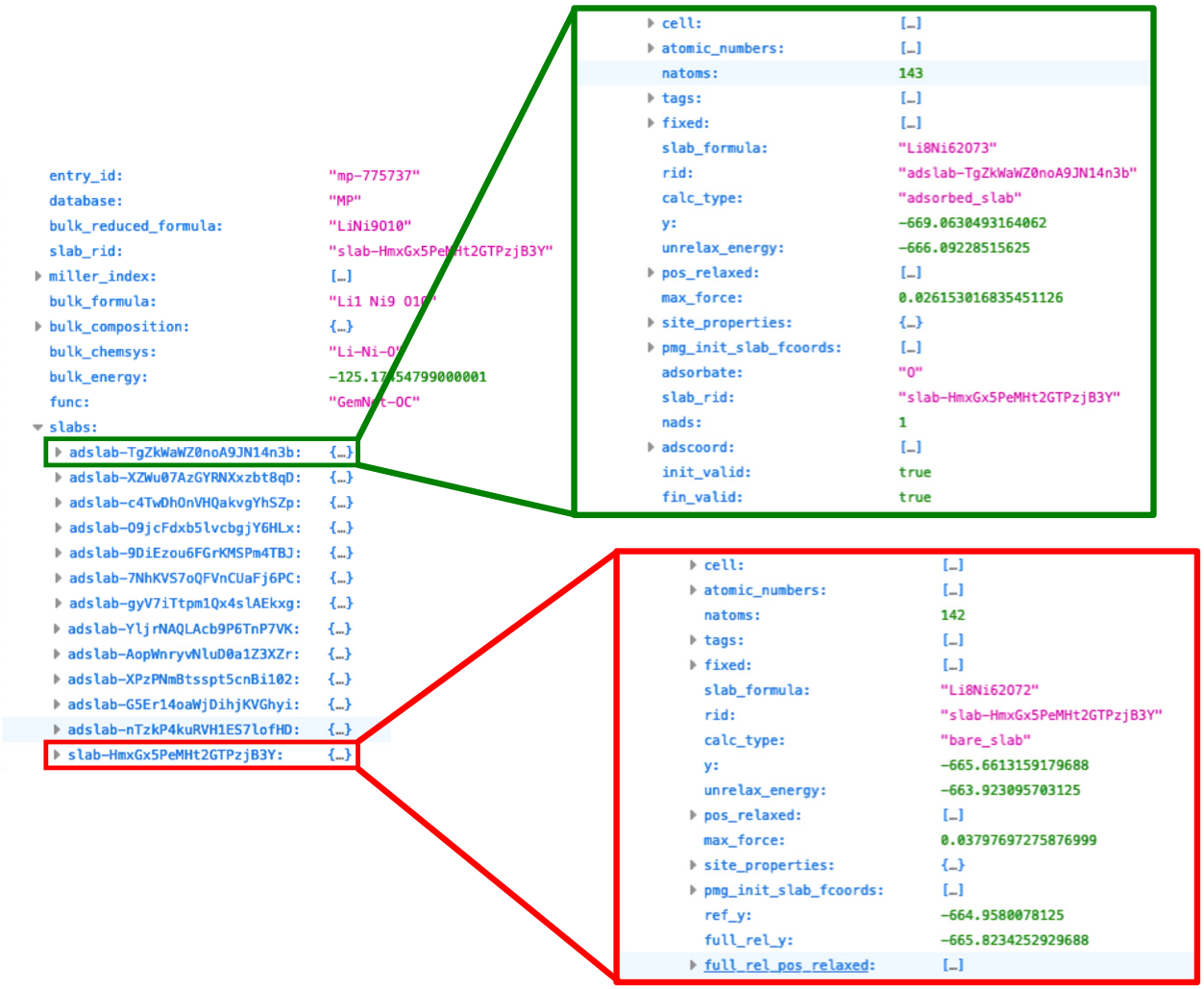


Figure 3: Dictionary object of a single entry in each database file.

Metadata of each surface includes the Materials Project ID (entry_id), the database

from which the bulk structure used to generate the slab was obtained from (database), the chemical formula of the bulk (bulk_reduced_formula), a unique 20 character random ID that is assigned to all slabs considered (slab_rid) with the 'slab-' prefix indicating a bare slab structure, the Miller index (miller_index), the formula of the conventional unit cell (bulk_formula), a *pymatgen* composition dictionary (bulk_composition), the chemical system (bulk_chemsys), the total energy of the DFT computed conventional bulk structure (bulk_energy), the ML architecture used to perform the predictions (func), and a dictionary containing additional information pertaining to each individual adsorbed slab derived from the bare slab (slabs).

The keys of the slabs dictionary are the unique 20 character random ID corresponding to each slab (designated with the 'slab-' prefix) and adsorbed slab (designated with the 'adslab-' prefix). Each value of the dictionary represents a single prediction of a slab or adsorbed slab and contains its predicted properties and metadata properties. These properties are the lattice parameter matrix of the slab (cell), a list of atomic numbers making up the slab (atomic_numbers), the number of atoms in the slab (natoms), tags indicating subsurface, surface and adsorbate atoms (tags), the index of atoms that were fixed during relaxation (fixed), the formula of the slab (slab_formula), the random ID (rid), the type of calculation (calc_type), the final energy (y), the unrelaxed energy (unrelax_energy), the reference slab energy used for calculating adsorption energy (ref_y) the relaxed xyz positions of all atoms in Cartesian coordinates (pos_relaxed), the maximum force during the final relaxation step (max_force), site properties such as the bulk Wyckoff positions (site_properties), and the fractional crystal coordinates of the initial structure (pmg_init_slab_fcoords). For entries corresponding to the adsorbed slabs, we also provided the random ID of the corresponding bare slab to help expedite binding energy calculations (slab_rid), the fractional coordinate position of the adsorbate (slab_rid) the intermediate (adsorbate), and the number of adsorbates (nads). As mentioned in the main manuscript, surfaces yielding low overpotentials of $\eta_{OER} < 0.75V$ are also fully relaxed without the application of spring forces to maintain

the intermediate identity an prevent desorption. These entries will have the relaxed energy (full_rel_y) and relaxed coordinates (full_rel_pos_relaxed).

# Candidate materials

Table 1: Summary of screening criteria for our final set of 190 candidate catalyst materials for OER across all screening frameworks with the formula, space group, number of facets on the Wulff shape with $\eta < 0.75$ V, lowest overpotential across the facets, the screening framework used to identify this candidate (See superscript labels in Table 2 of the main manuscript), the Pourbaix formation energy ($E_{PBX}$), energy above hull ($E_{hull}$), and material cost. Entries are sorted by $E_{PBX}$.

| Formula | Space group | # facets | $\eta$ (V) | Screening framework | $E_{PBX}$ (eV) | $E_{hull}$ (eV) | Cost ($/kg) |
|---|---|---|---|---|---|---|---|
| $HgSeO_4$ | $Pmn2_1$ | 2 | 0.18 | a,d,e,h,i,l,m,p | 0.00 | 0.00 | 65.47 |
| $Ni(BiO_3)_2$ | $P4_2/mnm$ | 4 | 0.36 | a,b,c,d,e,f,g,h i,j,k,l,m,n,o,p | 0.00 | 0.00 | 20.88 |
| $Na_2Se_2O_7$ | $P\bar{1}$ | 2 | 0.21 | a,d,e,h,i,l,m,p | 0.00 | 0.00 | 110.43 |
| $Ag_3O_4$ | $P2_1/c$ | 4 | 0.33 | a,b,c,d,e,f,g,h i,j,k,l,m,n,o,p | 0.00 | 0.00 | 714.77 |
| $PbO_2$ | $P4_2/mnm$ | 2 | 0.33 | a,d,e,h,i,l,m,p | 0.00 | 0.00 | 2.41 |
| $Mg(BiO_3)_2$ | $P4_2/mnm$ | 3 | 0.52 | a,b,c,d,e,f,g,h i,j,k,l,m,n,o,p | 0.00 | 0.00 | 20.41 |
| AgO | $Cccm$ | 2 | 0.49 | a,d,e,h,i,l,m,p | 0.00 | 0.00 | 745.41 |
| AgO | $C2/c$ | 2 | 0.51 | a,d,e,h,i,l,m,p | 0.01 | 0.01 | 745.41 |
| $PbO_2$ | $Pbcn$ | 2 | 0.56 | a,b,c,d,e,f,g,h i,j,k,l,m,n,o,p | 0.01 | 0.01 | 2.41 |
| $Co(BiO_3)_2$ | $P4_2/mnm$ | 2 | 0.33 | a,d,e,h,i,l,m,p | 0.02 | 0.02 | 24.34 |
| AgO | $P2_1/c$ | 3 | 0.50 | a,b,c,d,e,f,g,h i,j,k,l,m,n,o,p | 0.04 | 0.04 | 745.41 |
| $Bi_4O_7$ | $P\bar{1}$ | 2 | 0.22 | a,d,e,h,i,l,m,p | 0.04 | 0.00 | 22.67 |
| $FeCo_9O_{20}$ | $P\bar{1}$ | 4 | 0.41 | a,b,c,d,e,f,g,h i,j,k,l,m,n,o,p | 0.06 | 0.07 | 31.63 |
| $Ag_2SeO_4$ | $Fddd$ | 2 | 0.40 | a,b,c,d,e,f,g,h i,j,k,l,m,n,o,p | 0.07 | 0.00 | 547.23 |
| $Bi_3SbO_7$ | $P\bar{1}$ | 6 | 0.40 | a,b,c,d,e,f,g,h i,j,k,l,m,n,o,p | 0.07 | 0.00 | 20.85 |
| $CaBi_4O_9$ | $P2/c$ | 2 | 0.37 | a,d,e,h,i,l,m,p | 0.07 | 0.00 | 21.36 |
| $Li(CoO_2)_8$ | $P\bar{1}$ | 4 | 0.46 | a,b,c,d,e,f,g,h i,j,k,l,m,n,o,p | 0.08 | 0.03 | 34.60 |
| $LiSbO_3$ | $Pnna$ | 2 | 0.61 | a,b,c,d,e,f,g,h i,j,k,l,m,n,o,p | 0.09 | 0.00 | 10.82 |
| $CoAgO_3$ | $R\bar{3}$ | 2 | 0.31 | a,b,c,d,e,f,g,h i,j,k,l,m,n,o,p | 0.09 | 0.09 | 444.63 |
| $AgSnO_3$ | $Cmmm$ | 2 | 0.49 | a,d,e,h,i,l,m,p | 0.09 | 0.09 | 350.79 |

Table 2: Summary of screening criteria for our final set of candidates (continued).

| Formula | Space group | # facets | $\eta$ (V) | Screening framework | $E_{PBX}$ (eV) | $E_{hull}$ (eV) | Cost ($/kg) |
|---|---|---|---|---|---|---|---|
| $Na(CoO_2)_3$ | $C2/m$ | 3 | 0.42 | a,b,c,d,e,f,g,h i,j,k,l,m,n,o,p | 0.10 | 0.00 | 51.61 |
| $Ce_9YO_{20}$ | $P\bar{1}$ | 2 | 0.71 | a,d,e,h,i,l,m,p | 0.10 | 0.02 | 266.60 |
| $Ce_4SnO_{10}$ | $R\bar{3}m$ | 2 | 0.59 | a,b,c,d,e,f,g,h i,j,k,l,m,n,o,p | 0.11 | 0.07 | 239.03 |
| $Ag_6Mo_{10}O_{33}$ | $P\bar{1}$ | 3 | 0.55 | a,d,e,h,i,l,m,p | 0.11 | 0.02 | 278.69 |
| $CdGe_2O_5$ | $P\bar{1}$ | 2 | 0.42 | a,d,e,h,i,l,m,p | 0.11 | 0.01 | 625.43 |
| $CuMoO_4$ | $P\bar{1}$ | 6 | 0.46 | a,b,c,d,e,f,g,h i,j,k,l,m,n,o,p | 0.13 | 0.02 | 21.29 |
| $ReAgO_4$ | $I4_1/a$ | 2 | 0.49 | a,d,e,h,i,l,m,p | 0.13 | 0.00 | 1737.20 |
| $CuMoO_4$ | $P\bar{1}$ | 3 | 0.63 | a,b,c,d,e,f,g,h i,j,k,l,m,n,o,p | 0.15 | 0.04 | 21.29 |
| $Ce_2Mo_4O_{15}$ | $P\bar{1}$ | 4 | 0.46 | a,b,c,d,e,f,g,h i,j,k,l,m,n,o,p | 0.16 | 0.02 | 126.84 |
| $Ca(CuO_2)_2$ | $Pbcm$ | 2 | 0.60 | a,b,c,d,e,f,g,h i,j,k,l,m,n,o,p | 0.16 | 0.02 | 6.91 |
| $Cu_3Mo_2O_9$ | $P\bar{1}$ | 2 | 0.55 | a,d,e,h,i,l,m,p | 0.18 | 0.03 | 19.31 |
| $Ti_2CoO_5$ | $Cmcm$ | 2 | 0.58 | a,b,c,d,e,f,g,h i,j,k,l,m,n,o,p | 0.19 | 0.00 | 18.83 |
| $TlCoO_3$ | $R\bar{3}$ | 2 | 0.41 | a,b,c,d,e,f,g,h i,j,k,l,m,n,o,p | 0.19 | 0.05 | 3950.09 |
| $Mn(SbO_3)_2$ | $P321$ | 2 | 0.48 | a,b,c,d,e,f,g,h i,j,k,l,m,n,o,p | 0.20 | 0.00 | 9.84 |
| $CuWO_4$ | $P\bar{1}$ | 2 | 0.39 | a,b,c,d,e,f,g,h i,j,k,l,m,n,o,p | 0.20 | 0.08 | 23.40 |
| $NiBiO_3$ | $Pnma$ | 2 | 0.50 | a,b,c,d,e,f,g,h i,j,k,l,m,n,o,p | 0.21 | 0.04 | 20.66 |
| $Fe(Bi_5O_8)_5$ | $P23$ | 2 | 0.70 | a,d,e,h,i,l,m,p | 0.21 | 0.03 | 22.66 |
| $Cu_3(SbO_3)_4$ | $Im\bar{3}$ | 2 | 0.37 | a,d,e,h,i,l,m,p | 0.21 | 0.02 | 10.76 |
| $Bi_2O_3$ | $P2_1/c$ | 2 | 0.52 | a,d,e,h,i,l,m,p | 0.22 | 0.00 | 23.01 |
| $Cr_2Ag_2O_7$ | $P\bar{1}$ | 3 | 0.52 | a,b,c,d,e,f,g,h i,j,k,l,m,n,o,p | 0.22 | 0.02 | 430.56 |
| $Cr_2Ag_2O_7$ | $P\bar{1}$ | 3 | 0.43 | a,b,c,d,e,f,g,h i,j,k,l,m,n,o,p | 0.22 | 0.03 | 430.56 |
| $AlTlO_3$ | $Pnma$ | 2 | 0.55 | a,b,c,d,e,f,g,h i,j,k,l,m,n,o,p | 0.22 | 0.08 | 4391.10 |
| $LiAgO_2$ | $C2/m$ | 2 | 0.39 | a,d,e,h,i,l,m,p | 0.22 | 0.02 | 629.44 |

Table 3: Summary of screening criteria for our final set of candidates (continued).

| Formula | Space group | # facets | $\eta$ (V) | Screening framework | $E_{PBX}$ (eV) | $E_{hull}$ (eV) | Cost ($/kg) |
|---|---|---|---|---|---|---|---|
| $Nb_2Cu_3O_8$ | $P\bar{1}$ | 3 | 0.36 | a,b,c,d,e,f,g,h i,j,k,l,m,n,o,p | 0.23 | -7.61 | 19.94 |
| $Cd(CoO_2)_2$ | $Pmmn$ | 2 | 0.43 | a,b,c,d,e,f,g,h i,j,k,l,m,n,o,p | 0.23 | -6.26 | 22.61 |
| $Bi_2O_3$ | $Pbcn$ | 3 | 0.40 | a,b,c,d,e,f,g,h i,j,k,l,m,n,o,p | 0.24 | 0.02 | 23.01 |
| $Ag_2BiO_3$ | $Pnna$ | 3 | 0.34 | a,b,c,d,e,f,g,h i,j,k,l,m,n,o,p | 0.24 | 0.00 | 401.94 |
| $K(CoO_2)_2$ | $P2_1$ | 3 | 0.51 | a,b,c,d,e,f,g,h i,j,k,l,m,n,o,p | 0.24 | 0.00 | 205.67 |
| $ZnCoO_3$ | $C2/c$ | 2 | 0.49 | a,d,e,h,i,l,m,p | 0.25 | 0.06 | 19.81 |
| $Li(Bi_3O_5)_4$ | $I23$ | 2 | 0.47 | a,d,e,h,i,l,m,p | 0.25 | 0.08 | 22.74 |
| $CoAgO_2$ | $P6_3/mmc$ | 2 | 0.47 | a,b,c,d,e,f,g,h i,j,k,l,m,n,o,p | 0.26 | 0.00 | 480.17 |
| $Cu(BiO_2)_2$ | $P4/ncc$ | 3 | 0.41 | a,b,c,d,e,f,g,h i,j,k,l,m,n,o,p | 0.26 | 0.01 | 20.85 |
| $CdCoO_3$ | $C2/c$ | 2 | 0.46 | a,d,e,h,i,l,m,p | 0.28 | 0.05 | 16.08 |
| $Cd_2PbO_4$ | $Pbam$ | 3 | 0.22 | a,b,c,d,e,f,g,h i,j,k,l,m,n,o,p | 0.29 | 0.00 | 2.59 |
| $Ag_2GeO_3$ | $P2_12_12_1$ | 2 | 0.62 | a,d,e,h,i,l,m,p | 0.29 | 0.00 | 862.25 |
| $MnMoO_5$ | $P\bar{1}$ | 2 | 0.56 | a,d,e,h,i,l,m,p | 0.30 | -8.27 | 18.68 |
| $ScCoO_3$ | $P2_1/c$ | 2 | 0.34 | a,b,c,d,e,f,g,h i,j,k,l,m,n,o,p | 0.30 | 0.06 | 1045.31 |
| $Mn(SeO_3)_2$ | $P2_1/c$ | 4 | 0.35 | a,b,c,d,e,f,g,h i,j,k,l,m,n,o,p | 0.31 | 0.00 | 75.94 |
| $Cr_3AgO_8$ | $C2/m$ | 2 | 0.62 | a,b,c,d,e,f,g,h i,j,k,l,m,n,o,p | 0.32 | 0.00 | 240.23 |
| $InCoO_3$ | $Pnma$ | 2 | 0.58 | a,b,c,d,e,f,g,h i,j,k,l,m,n,o,p | 0.32 | 0.07 | 387.34 |
| $Ca(FeO_2)_2$ | $Pm$ | 2 | 0.59 | a,d,e,h,i,l,m,p | 0.33 | 0.01 | 1.90 |
| $MnO_2$ | $Pnma$ | 2 | 0.41 | a,b,c,d,i,j,k,l | 0.33 | 0.00 | 2.41 |
| $TiAg_2O_3$ | $C2/c$ | 2 | 0.47 | a,d,e,h,i,l,m,p | 0.33 | 0.04 | 594.55 |
| $CoPbO_3$ | $R\bar{3}$ | 3 | 0.36 | a,d,e,h,i,l,m,p | 0.34 | 0.03 | 11.78 |
| $CaBiO_3$ | $P2_1/c$ | 3 | 0.35 | a,b,c,d,e,f,g,h i,j,k,l,m,n,o,p | 0.34 | 0.00 | 18.94 |
| $Tl_3Co_3O_8$ | $P1$ | 2 | 0.50 | a,d,e,h,i,l,m,p | 0.35 | 0.07 | 4018.88 |

Table 4: Summary of screening criteria for our final set of candidates (continued).

| Formula | Space group | # facets | $\eta$ (V) | Screening framework | $E_{PBX}$ (eV) | $E_{hull}$ (eV) | Cost ($/kg) |
|---|---|---|---|---|---|---|---|
| $SrBiO_3$ | $P2_1/c$ | 3 | 0.39 | a,b,c,d,e,f,g,h i,j,k,l,m,n,o,p | 0.35 | 0.00 | 16.06 |
| $Ce_{11}O_{20}$ | $P\bar{1}$ | 4 | 0.32 | a,b,c,d,e,f,g,h i,j,k,l,m,n,o,p | 0.35 | 0.00 | 290.42 |
| $NaBi_5O_8$ | $P\bar{1}$ | 3 | 0.52 | a,b,c,d,e,f,g,h i,j,k,l,m,n,o,p | 0.35 | 0.03 | 27.24 |
| $TlBiO_4$ | $Cmmm$ | 2 | 0.33 | a,d,i,l | 0.36 | -5.53 | 2580.81 |
| $Cu_4Se_3O_{10}$ | $P\bar{1}$ | 2 | 0.52 | a,d,e,h,i,l,m,p | 0.36 | 0.02 | 57.57 |
| $BaBiO_3$ | $P2_1/c$ | 2 | 0.63 | a,d,e,h,i,l,m,p | 0.36 | 0.00 | 13.87 |
| $Ce_2(GeO_3)_3$ | $P\bar{1}$ | 2 | 0.55 | a,b,c,d,e,f,g,h i,j,k,l,m,n,o,p | 0.36 | 0.05 | 645.52 |
| $CdSe_2O_5$ | $C2/c$ | 2 | 0.66 | a,d,e,h,i,l,m,p | 0.36 | 0.00 | 67.37 |
| $AgBiO_2$ | $P2_1/m$ | 3 | 0.55 | a,b,c,d,e,f,g,h i,j,k,l,m,n,o,p | 0.36 | 0.00 | 279.98 |
| $Zn(BiO_2)_2$ | $P\bar{1}$ | 3 | 0.43 | a,b,c,d,e,f,g,h i,j,k,l,m,n,o,p | 0.36 | 0.07 | 20.03 |
| $CuSeO_3$ | $P2_1/c$ | 4 | 0.41 | a,b,c,d,e,f,g,h i,j,k,l,m,n,o,p | 0.37 | 0.03 | 64.44 |
| $Cu_2SeO_4$ | $P2_1/c$ | 4 | 0.38 | a,b,c,d,e,f,g,h i,j,k,l,m,n,o,p | 0.37 | 0.03 | 47.88 |
| $CdSeO_3$ | $Pnma$ | 4 | 0.49 | a,b,c,d,e,f,g,h i,j,k,l,m,n,o,p | 0.37 | 0.01 | 50.04 |
| $FeSnO_3$ | $P\bar{1}$ | 2 | 0.51 | a,b,c,d,e,f,g,h i,j,k,l,m,n,o,p | 0.38 | 0.00 | 18.17 |
| $CoGeO_3$ | $C2/c$ | 3 | 0.50 | a,b,c,d,e,f,g,h i,j,k,l,m,n,o,p | 0.38 | 0.06 | 604.48 |
| $Hg_2MoO_4$ | $C2/c$ | 2 | 0.26 | a,d,e,h,i,l,m,p | 0.38 | 0.01 | 45.80 |
| $CdIn_2O_4$ | $Imma$ | 2 | 0.46 | a,b,c,d,e,f,g,h i,j,k,l,m,n,o,p | 0.38 | 0.08 | 408.44 |
| $BaTl_2O_4$ | $Pnma$ | 3 | 0.54 | a,b,c,d,e,f,g,h i,j,k,l,m,n,o,p | 0.38 | 0.00 | 4021.08 |
| $Cr(SbO_3)_2$ | $Pnnm$ | 2 | 0.39 | a,b,c,d,e,f,g,h i,j,k,l,m,n,o,p | 0.38 | 0.06 | 10.88 |
| $Li_3BiO_4$ | $P2/c$ | 2 | 0.41 | a,b,c,d,i,j,k,l | 0.38 | 0.00 | 18.93 |
| $SrSe_2O_5$ | $P\bar{1}$ | 3 | 0.25 | a,b,c,d,e,f,g,h i,j,k,l,m,n,o,p | 0.39 | 0.00 | 71.87 |
| $Ca_2Se_3O_8$ | $P\bar{1}$ | 2 | 0.70 | a,d,e,h,i,l,m,p | 0.39 | 0.00 | 79.44 |

Table 5: Summary of screening criteria for our final set of candidates (continued).

| Formula | Space group | # facets | $\eta$ (V) | Screening framework | $E_{PBX}$ (eV) | $E_{hull}$ (eV) | Cost ($/kg) |
|---|---|---|---|---|---|---|---|
| $Cd_6(CoO_3)_5$ | $R32$ | 2 | 0.39 | a,b,c,d,e,f,g,h i,j,k,l,m,n,o,p | 0.39 | 0.09 | 14.84 |
| $Ag_2SeO_3$ | $P2_1/c$ | 3 | 0.29 | a,b,c,d,g,h,i,j k,l,o,p | 0.40 | 0.00 | 572.64 |
| $BaSe_2O_5$ | $P2_1/c$ | 2 | 0.66 | a,d,e,h,i,l,m,p | 0.40 | 0.00 | 62.17 |
| $LuCoO_3$ | $Pnma$ | 2 | 0.56 | a,b,c,d,e,f,g,h i,j,k,l,m,n,o,p | 0.40 | 0.03 | 4666.55 |
| $Ag_4GeO_4$ | $P\bar{1}$ | 6 | 0.52 | a,b,c,d,e,f,g,h i,j,k,l,m,n,o,p | 0.40 | 0.01 | 835.50 |
| $CuReO_4$ | $P\bar{1}$ | 4 | 0.33 | a,b,c,d,e,f,g,h i,j,k,l,m,n,o,p | 0.40 | 0.06 | 1690.40 |
| $Co_{11}CuO_{16}$ | $P2/m$ | 2 | 0.56 | a,d,i,l | 0.40 | 0.06 | 36.39 |
| $CoSe_2O_5$ | $Pbcn$ | 2 | 0.40 | a,b,c,d | 0.41 | 0.00 | 88.84 |
| $Co_5SbO_8$ | $R\bar{3}m$ | 2 | 0.49 | a,b,c,d,i,j,k,l | 0.41 | 0.00 | 32.16 |
| $NaTlO_2$ | $I4_1/amd$ | 2 | 0.49 | a,d,e,h,i,l,m,p | 0.41 | 0.02 | 4751.26 |
| $MgIn_2O_4$ | $Imma$ | 2 | 0.42 | a,b,c,d,e,f,g,h i,j,k,l,m,n,o,p | 0.41 | 0.02 | 521.03 |
| $Li_7Co_5O_{12}$ | $C2/m$ | 4 | 0.38 | a,b,c,d,e,f,g,h i,j,k,l,m,n,o,p | 0.41 | 0.03 | 30.17 |
| $Hg_2WO_4$ | $C2/c$ | 2 | 0.68 | a,d,e,h,i,l,m,p | 0.42 | 0.00 | 43.49 |
| $CuReO_4$ | $P\bar{1}$ | 3 | 0.56 | a,b,c,d,e,f,g,h i,j,k,l,m,n,o,p | 0.42 | 0.08 | 1690.40 |
| $Sn_2Ge_2O_7$ | $P\bar{1}$ | 2 | 0.55 | a,d,e,h,i,l,m,p | 0.42 | 0.06 | 442.22 |
| $MnTlO_3$ | $Pnma$ | 5 | 0.20 | a,b,c,d,i,j,k,l | 0.42 | 0.05 | 3991.79 |
| $Ag_2HgO_2$ | $P4_32_12$ | 3 | 0.47 | a,b,c,d,g,h,i,j k,l,o,p | 0.43 | 0.00 | 435.93 |
| $Co_2NiO_4$ | $Imma$ | 2 | 0.50 | a,b,c,d,e,f,g,h i,j,k,l,m,n,o,p | 0.43 | 0.09 | 30.91 |
| $Ba_8(Bi_2O_7)_3$ | $P\bar{1}$ | 6 | 0.46 | a,b,c,d,i,j,k,l | 0.43 | 0.00 | 12.29 |
| $AgSbO_4$ | $Cmmm$ | 3 | 0.32 | a,b,c,d,i,j,k,l | 0.44 | -5.61 | 320.88 |
| $MnTlO_3$ | $P\bar{1}$ | 3 | 0.36 | a,b,c,d,i,j,k,l | 0.44 | 0.07 | 3991.79 |
| $Ca(CoO_2)_2$ | $Pnma$ | 2 | 0.32 | a,b,c,d,e,f,g,h i,j,k,l,m,n,o,p | 0.44 | 0.00 | 29.47 |
| $Tl_2SeO_4$ | $Pnma$ | 3 | 0.58 | a,b,c,d,i,j,k,l | 0.45 | 0.00 | 4467.30 |
| $Tl_2SeO_4$ | $P2_12_12_1$ | 4 | 0.52 | a,b,c,d,i,j,k,l | 0.45 | 0.00 | 4467.30 |
| $CaSeO_3$ | $Pnma$ | 2 | 0.60 | a,b,c,d,g,h,i,j k,l,o,p | 0.45 | 0.01 | 71.04 |

Table 6: Summary of screening criteria for our final set of candidates (continued).

| Formula | Space group | # facets | $\eta$ (V) | Screening framework | $E_{PBX}$ (eV) | $E_{hull}$ (eV) | Cost ($/kg) |
|---|---|---|---|---|---|---|---|
| $CdCu_2O_3$ | $Pmmn$ | 2 | 0.50 | a,b,c,d,g,h,i,j k,l,o,p | 0.46 | 0.04 | 5.78 |
| $CuSbO_4$ | $Cmmm$ | 2 | 0.36 | a,b,c,d,i,j,k,l | 0.47 | -6.01 | 10.18 |
| $YMn_2O_5$ | $Pbam$ | 2 | 0.54 | a,b,c,d,i,j,k,l | 0.47 | 0.00 | 11.56 |
| $Cu_2W_2O_7$ | $P\bar{1}$ | 2 | 0.43 | a,b,c,d,i,j,k,l | 0.47 | 0.10 | 23.94 |
| $Ca_3WO_6$ | $P2_1/c$ | 2 | 0.49 | a,d,e,h,i,l,m,p | 0.47 | 0.02 | 18.40 |
| $YCoO_3$ | $P2_1/c$ | 2 | 0.52 | a,b,c,d,i,j,k,l | 0.48 | 0.01 | 30.52 |
| $ZnCu_2O_3$ | $Pmmn$ | 3 | 0.42 | a,b,c,d,g,h,i,j k,l,o,p | 0.48 | 0.10 | 6.44 |
| $CuNiO_2$ | $C2/m$ | 2 | 0.40 | a,b,c,d,i,j,k,l | 0.49 | 0.07 | 11.60 |
| $MnBiO_3$ | $Pnma$ | 3 | 0.51 | a,b,c,d,k,l | 0.50 | 0.03 | 17.78 |

Table 7: Summary of screening criteria for our final set of candidates (continued). All materials listed from here are unstable as bulk materials ($E_{PBX} > 0.5$ eV) but can be stabilized as nanoparticles.

| Formula | Space group | # facets | $\eta$ (V) | Screening framework | $E_{PBX}$ (eV) | $E_{hull}$ (eV) | Cost ($/kg) |
|---|---|---|---|---|---|---|---|
| $Cr_2WO_6$ | $P4_2/mnm$ | 2 | 0.25 | c,d,k,l | 0.52 | 0.00 | 20.20 |
| $TlCuO_2$ | $R\bar{3}m$ | 2 | 0.43 | h,p | 0.52 | 0.05 | 4091.65 |
| $Y(FeO_2)_2$ | $P\bar{1}$ | 2 | 0.53 | c,d,g,h,k,l,o,p | 0.54 | 0.01 | 11.23 |
| $Sr_2Tl_2O_5$ | $P2_1/c$ | 2 | 0.37 | k,l | 0.55 | 0.00 | 3694.92 |
| $ZrCoO_3$ | $P\bar{1}$ | 3 | 0.46 | c,d,g,h,k,l,o,p | 0.55 | 0.10 | 32.83 |
| $TiVO_4$ | $P2_1$ | 2 | 0.58 | c,d,k,l | 0.56 | 0.02 | 120.33 |
| $HfFeO_3$ | $Pnma$ | 2 | 0.53 | c,d,k,l | 0.56 | 0.06 | 569.53 |
| $Mn_4CuO_8$ | $C2/m$ | 3 | 0.39 | d,l | 0.56 | 0.07 | 3.51 |
| $CoCu_2O_3$ | $Pmmn$ | 3 | 0.42 | c,d,k,l | 0.57 | 0.07 | 18.94 |
| $MnSe_2O_5$ | $Pbcn$ | 2 | 0.50 | c,d,k,l | 0.58 | 0.00 | 79.93 |
| $CrMoO_4$ | $Cmmm$ | 2 | 0.42 | c,d,k,l | 0.59 | 0.00 | 21.89 |
| $KMn_2O_4$ | $P\bar{1}$ | 2 | 0.47 | d,l | 0.60 | 0.00 | 185.55 |
| $Ba_2Tl_2O_5$ | $Pnma$ | 2 | 0.34 | d,l | 0.60 | 0.00 | 3213.59 |
| $LuMnO_3$ | $Pnma$ | 3 | 0.54 | c,d,g,h,k,l,o,p | 0.61 | 0.05 | 4722.98 |
| $TiMnO_3$ | $R\bar{3}$ | 2 | 0.28 | d,l | 0.62 | 0.00 | 5.36 |
| $KBiO_2$ | $C2/c$ | 2 | 0.27 | c,d,k,l | 0.62 | 0.00 | 158.83 |
| $Na_5ReO_6$ | $C2/m$ | 2 | 0.30 | h,l,p | 0.62 | 0.00 | 1406.49 |
| $CuTeO_4$ | $Cmmm$ | 3 | 0.54 | c,d,k,l | 0.63 | -5.71 | 177.66 |
| $ScCrO_3$ | $Pnma$ | 2 | 0.46 | c,d,g,h,k,l,o,p | 0.63 | 0.04 | 1077.47 |
| $Ta_2CrO_6$ | $P4_2/mnm$ | 2 | 0.56 | c,d,k,l | 0.64 | 0.01 | 109.26 |
| $MnSnO_3$ | $R\bar{3}$ | 2 | 0.43 | c,d,k,l | 0.65 | 0.00 | 18.71 |
| $Li_4PbO_4$ | $Cmcm$ | 2 | 0.66 | d,l | 0.65 | 0.00 | 2.61 |
| $VSbO_4$ | $Cmmm$ | 2 | 0.44 | d,h,l,p | 0.66 | 0.02 | 87.80 |
| $ScCuO_2$ | $R\bar{3}m$ | 2 | 0.41 | d,h,l,p | 0.66 | 0.00 | 1112.09 |
| $Mn_2BeO_4$ | $Pnma$ | 3 | 0.32 | c,d,g,h,k,l,o,p | 0.66 | 0.04 | 24.36 |
| $AlCuO_2$ | $P6_3/mmc$ | 2 | 0.48 | c,d,k,l,o,p | 0.67 | 0.00 | 6.28 |
| $TiCu_3O_4$ | $P2_1/c$ | 2 | 0.38 | g,h,o,p | 0.68 | 0.07 | 8.46 |
| $Ag_2PbO_2$ | $C2/c$ | 3 | 0.43 | g,h,o,p | 0.70 | 0.00 | 406.97 |
| $LuCrO_3$ | $Pnma$ | 2 | 0.43 | c,d,g,h,k,l,o,p | 0.71 | 0.00 | 4774.87 |
| $VSeO_4$ | $P2_1/c$ | 2 | 0.46 | d,l | 0.72 | 0.00 | 157.65 |
| $Ag_3RuO_4$ | $P4_122$ | 2 | 0.60 | d,l | 0.72 | 0.07 | 5554.14 |
| $GePb_5O_7$ | $Pbca$ | 2 | 0.68 | g,h,k,l,o,p | 0.72 | 0.01 | 88.53 |
| $VCrO_4$ | $Cmcm$ | 2 | 0.32 | c,d | 0.73 | 0.01 | 116.99 |
| $TlTeO_4$ | $Cmmm$ | 2 | 0.50 | c,d,k,l | 0.74 | -5.50 | 3210.31 |
| $MnSeO_3$ | $P2_1/c$ | 2 | 0.44 | c,d,k,l | 0.75 | 0.00 | 64.79 |
| $Li_3BiO_3$ | $P\bar{1}$ | 2 | 0.52 | d,h,l,p | 0.75 | 0.00 | 19.85 |
| $VZn_2O_4$ | $Imma$ | 2 | 0.47 | k,l | 0.75 | 0.02 | 79.05 |
| $Fe_{10}O_{11}$ | $P\bar{1}$ | 3 | 0.50 | g,h,o,p | 0.77 | 0.05 | 0.88 |

Table 8: Summary of screening criteria for our final set of candidates (continued).

| Formula | Space group | # facets | $\eta$ (V) | Screening framework | $E_{PBX}$ (eV) | $E_{hull}$ (eV) | Cost ($/kg) |
|---|---|---|---|---|---|---|---|
| $Tl_2SnO_3$ | $Pnma$ | 2 | 0.60 | d,h | 0.80 | 0.00 | 4269.57 |
| $ScMn_2O_4$ | $C2/m$ | 3 | 0.29 | k,l | 0.84 | 0.03 | 712.73 |
| $ZrMnO_3$ | $R\bar{3}$ | 2 | 0.50 | c,d,g,h,k,l,o,p | 0.84 | 0.03 | 18.24 |
| $Li(CuO)_2$ | $Pnma$ | 2 | 0.52 | k,l | 0.85 | 0.00 | 8.03 |
| $Fe_{17}O_{18}$ | $P\bar{1}$ | 2 | 0.52 | l | 0.86 | 0.04 | 0.86 |
| $K_6Co_2O_7$ | $P2_1/c$ | 4 | 0.36 | c,d,k,l | 0.87 | 0.00 | 519.06 |
| $Cr_2NiO_4$ | $P1$ | 3 | 0.38 | d,h,l,p | 0.88 | 0.04 | 9.96 |
| $YCuO_2$ | $P6_3/mmc$ | 2 | 0.38 | k,l | 0.94 | 0.00 | 18.75 |
| $Mn_2SnO_4$ | $Imma$ | 3 | 0.42 | c,d,g,h,k,l,o,p | 0.94 | 0.00 | 14.72 |
| $MnCuO_2$ | $P\bar{1}$ | 2 | 0.58 | l | 0.94 | 0.00 | 5.41 |
| $YCuO_2$ | $R\bar{3}m$ | 2 | 0.38 | g,h,o,p | 0.94 | 0.00 | 18.75 |
| $Mn_{23}FeO_{32}$ | $P\bar{1}$ | 2 | 0.28 | d,h,l,p | 0.95 | 0.01 | 2.27 |
| $SrCr_2O_4$ | $Pmmn$ | 3 | 0.62 | c,d,k,l | 0.98 | 0.00 | 4.97 |
| $KSnO_2$ | $P\bar{1}$ | 2 | 0.19 | c,d,g,h,k,l,o,p | 0.98 | 0.02 | 226.98 |
| $CdRuO_4$ | $Cmmm$ | 2 | 0.53 | d,l | 0.99 | -6.31 | 8784.84 |
| $Co(SbO_2)_2$ | $P4_2/mbc$ | 2 | 0.66 | k,l | 0.99 | 0.00 | 18.42 |
| $Mn_2CrO_4$ | $Cc$ | 2 | 0.37 | c,d,k,l | 1.04 | 0.00 | 4.02 |
| $Na_2Sb_4O_7$ | $C2/c$ | 2 | 0.35 | k,l | 1.05 | 0.00 | 29.14 |
| $CeCrO_3$ | $Pnma$ | 2 | 0.29 | c,d,g,h,k,l,o,p | 1.05 | 0.05 | 206.93 |
| $Na_2Co_2O_3$ | $P2_1/c$ | 4 | 0.30 | g,h,o,p | 1.07 | 0.00 | 83.99 |
| $NaSb_5O_8$ | $P\bar{1}$ | 3 | 0.52 | k,l | 1.09 | 0.00 | 19.53 |
| $RuPbO_4$ | $Cmmm$ | 2 | 0.64 | d,l | 1.12 | -6.84 | 6548.46 |
| $SnRuO_4$ | $Cmmm$ | 2 | 0.32 | c,d,k,l | 1.14 | -7.30 | 8602.47 |
| $Ti(SnO_2)_2$ | $P4_2/mbc$ | 2 | 0.48 | k,l | 1.15 | 0.00 | 24.39 |
| $LiMn_3O_4$ | $P\bar{1}$ | 2 | 0.63 | d,l | 1.26 | 0.02 | 2.37 |
| $K_2PbO_2$ | $P\bar{1}$ | 2 | 0.55 | k,l | 1.31 | 0.00 | 248.19 |
| $Mn_2NiO_3$ | $Immm$ | 2 | 0.47 | d,h,l,p | 1.34 | 0.08 | 6.73 |
| $Mn_3NiO_4$ | $Cmmm$ | 2 | 0.54 | d,l | 1.44 | 0.09 | 5.63 |
| $BaMn_2O_3$ | $Immm$ | 2 | 0.62 | k,l | 1.66 | 0.00 | 1.38 |
| $CaMn_7O_8$ | $C2/m$ | 2 | 0.48 | l | 1.66 | 0.03 | 2.48 |

# Candidate materials literature references

Table 9: Overpotentials from OC22, the experimental literature, and DFT (see Figure 7(b) in the main manuscript) along with the potential determining step (PDS) for our final set of 190 candidate catalyst materials for OER across all screening frameworks. Experimental results are reported for systems containing similar chemical systems and do not necessarily reflect the same formula of the candidate catalyst. Candidates are listed in the same order as Tables S1-8 (from lowest to highest $E_{PBX}$).

| Formula | $\eta$ (V) (OC22) | $\eta$ (V) (exp.) | $\eta$ (V) (DFT) | PDS |
|---|---|---|---|---|
| $HgSeO_4$ | 0.176 | | 0.217 | $OH \longrightarrow O^{*+}H^+$ |
| $Ni(BiO_3)_2$ | 0.361 | 0.300[7] | | $OH \longrightarrow O^{*+}H^+$ |
| $Na_2Se_2O_7$ | 0.208 | | 0.741 | $OH \longrightarrow O^{*+}H^+$ |
| $Ag_3O_4$ | 0.333 | 0.37[8] | | $OH \longrightarrow O^{*+}H^+$ |
| $PbO_2$ | 0.334 | | | $OH \longrightarrow O^{*+}H^+$ |
| $Mg(BiO_3)_2$ | 0.525 | | | $OH \longrightarrow O^{*+}H^+$ |
| AgO | 0.495 | 0.37[8] | | $H_2O^+O^* \longrightarrow OOH^{*+}H^+$ |
| AgO | 0.513 | 0.37[8] | | $H_2O^+O^* \longrightarrow OOH^{*+}H^+$ |
| $PbO_2$ | 0.561 | | | $H_2O^+O^* \longrightarrow OOH^{*+}H^+$ |
| $Co(BiO_3)_2$ | 0.331 | 0.320[9] | | $OH \longrightarrow O^{*+}H^+$ |
| AgO | 0.496 | 0.37[8] | | $H_2O^+O^* \longrightarrow OOH^{*+}H^+$ |
| $Bi_4O_7$ | 0.221 | 0.800[10] | 0.353 | $OH \longrightarrow O^{*+}H^+$ |
| $FeCo_9O_{20}$ | 0.412 | 0.408,[11] 0.412[12] | | $H_2O^+O^* \longrightarrow OOH^{*+}H^+$ |
| $Ag_2SeO_4$ | 0.395 | 0.192[13] | | $H_2O^+O^* \longrightarrow OOH^{*+}H^+$ |
| $Bi_3SbO_7$ | 0.398 | | | $OH \longrightarrow O^{*+}H^+$ |
| $CaBi_4O_9$ | 0.368 | | | $OH \longrightarrow O^{*+}H^+$ |
| $Li(CoO_2)_8$ | 0.459 | 0.430[14] | | $OH \longrightarrow O^{*+}H^+$ |
| $LiSbO_3$ | 0.611 | | | $H_2O^+O^* \longrightarrow OOH^{*+}H^+$ |
| $CoAgO_3$ | 0.306 | 0.310[15] | | $OH \longrightarrow O^{*+}H^+$ |
| $AgSnO_3$ | 0.491 | | | $OH \longrightarrow O^{*+}H^+$ |
| $Na(CoO_2)_3$ | 0.416 | 0.236[16] | | $OH \longrightarrow O^{*+}H^+$ |
| $Ce_9YO_{20}$ | 0.705 | | | $OH \longrightarrow O^{*+}H^+$ |
| $Ce_4SnO_{10}$ | 0.594 | | | $H_2O^+O^* \longrightarrow OOH^{*+}H^+$ |
| $Ag_6Mo_{10}O_{33}$ | 0.546 | $> 0.540$[17] | | $OH \longrightarrow O^{*+}H^+$ |
| $CdGe_2O_5$ | 0.423 | | | $OH \longrightarrow O^{*+}H^+$ |
| $CuMoO_4$ | 0.460 | | | $OH \longrightarrow O^{*+}H^+$ |
| $ReAgO_4$ | 0.488 | | | $OH \longrightarrow O^{*+}H^+$ |
| $CuMoO_4$ | 0.626 | | | $OH \longrightarrow O^{*+}H^+$ |
| $Ce_2Mo_4O_{15}$ | 0.463 | | | $OH \longrightarrow O^{*+}H^+$ |
| $Ca(CuO_2)_2$ | 0.598 | | | $H_2O^+O^* \longrightarrow OOH^{*+}H^+$ |
| $Cu_3Mo_2O_9$ | 0.545 | | | $OH \longrightarrow O^{*+}H^+$ |
| $Ti_2CoO_5$ | 0.577 | 0.66[18] | | $OH \longrightarrow O^{*+}H^+$ |

Table 10: Overpotentials from OC22, the experimental literature, and DFT (see Figure 7(b) in the main manuscript) along with the PDS for our final set of 190 candidate (continued).

| Formula | $\eta$ (V) (OC22) | $\eta$ (V) (exp.) | $\eta$ (V) (DFT) | PDS |
|---|---|---|---|---|
| $TlCoO_3$ | 0.407 | | | $H_2O^+O^* \longrightarrow OOH^{*+}H^+$ |
| $Mn(SbO_3)_2$ | 0.484 | 0.340[19] | | $OOH^* \longrightarrow O_2{}^+H^+$ |
| $CuWO_4$ | 0.391 | 0.270[20] | | $OH \longrightarrow O^{*+}H^+$ |
| $NiBiO_3$ | 0.504 | 0.300[7] | | $H_2O^+O^* \longrightarrow OOH^{*+}H^+$ |
| $Fe(Bi_5O_8)_5$ | 0.699 | 0.420[21] | | $H_2O^+O^* \longrightarrow OOH^{*+}H^+$ |
| $Cu_3(SbO_3)_4$ | 0.366 | | | $OH \longrightarrow O^{*+}H^+$ |
| $Bi_2O_3$ | 0.524 | 0.800[10] | 0.292 | $OH \longrightarrow O^{*+}H^+$ |
| $Cr_2Ag_2O_7$ | 0.522 | $> 0.540$[17] | | $H_2O^+O^* \longrightarrow OOH^{*+}H^+$ |
| $Cr_2Ag_2O_7$ | 0.426 | $> 0.540$[17] | | $H_2O^+O^* \longrightarrow OOH^{*+}H^+$ |
| $AlTlO_3$ | 0.553 | | | $OH \longrightarrow O^{*+}H^+$ |
| $LiAgO_2$ | 0.388 | | | $OH \longrightarrow O^{*+}H^+$ |
| $Nb_2Cu_3O_8$ | 0.363 | | | $OH \longrightarrow O^{*+}H^+$ |
| $Cd(CoO_2)_2$ | 0.431 | | | $OH \longrightarrow O^{*+}H^+$ |
| $Bi_2O_3$ | 0.396 | 0.800[10] | | $H_2O^+O^* \longrightarrow OOH^{*+}H^+$ |
| $Ag_2BiO_3$ | 0.343 | 0.700[22] | | $OH \longrightarrow O^{*+}H^+$ |
| $K(CoO_2)_2$ | 0.510 | | | $OOH^* \longrightarrow O_2{}^+H^+$ |
| $ZnCoO_3$ | 0.488 | $< 0.400$,[23] 0.390-0.480[24] | | $OH \longrightarrow O^{*+}H^+$ |
| $Li(Bi_3O_5)_4$ | 0.473 | | | $OOH^* \longrightarrow O_2{}^+H^+$ |
| $CoAgO_2$ | 0.472 | 0.310[15] | | $OH \longrightarrow O^{*+}H^+$ |
| $Cu(BiO_2)_2$ | 0.406 | 0.530[25] | | $H_2O^+O^* \longrightarrow OOH^{*+}H^+$ |
| $CdCoO_3$ | 0.459 | | | $OH \longrightarrow O^{*+}H^+$ |
| $Cd_2PbO_4$ | 0.220 | | 0.222 | $OH \longrightarrow O^{*+}H^+$ |
| $Ag_2GeO_3$ | 0.616 | | | $OOH^* \longrightarrow O_2{}^+H^+$ |
| $MnMoO_5$ | 0.564 | 0.570[26] | | $OH \longrightarrow O^{*+}H^+$ |
| $ScCoO_3$ | 0.341 | | | $OH \longrightarrow O^{*+}H^+$ |
| $Mn(SeO_3)_2$ | 0.349 | | | $OH \longrightarrow O^{*+}H^+$ |
| $Cr_3AgO_8$ | 0.620 | $> 0.540$[17] | | $H_2O^+O^* \longrightarrow OOH^{*+}H^+$ |
| $InCoO_3$ | 0.582 | 0.370[27] | | $OH \longrightarrow O^{*+}H^+$ |
| $Ca(FeO_2)_2$ | 0.586 | 0.320[28] | | $OH \longrightarrow O^{*+}H^+$ |
| $MnO_2$ | 0.406 | $> 0.600$[29] | | $OOH^* \longrightarrow O_2{}^+H^+$ |
| $TiAg_2O_3$ | 0.468 | 0.650[30] | | $H_2O^+O^* \longrightarrow OOH^{*+}H^+$ |
| $CoPbO_3$ | 0.356 | 0.560[31] | | $OH \longrightarrow O^{*+}H^+$ |
| $CaBiO_3$ | 0.352 | | | $OH \longrightarrow O^{*+}H^+$ |
| $Tl_3Co_3O_8$ | 0.503 | | | $H_2O^+O^* \longrightarrow OOH^{*+}H^+$ |
| $SrBiO_3$ | 0.392 | | | $OH \longrightarrow O^{*+}H^+$ |
| $Ce_{11}O_{20}$ | 0.324 | 0.370[32] | | $OOH^* \longrightarrow O_2{}^+H^+$ |

Table 11: Overpotentials from OC22, the experimental literature, and DFT (see Figure 7(b) in the main manuscript) along with the PDS for our final set of 190 candidate (continued).

| Formula | $\eta$ (V) (OC22) | $\eta$ (V) (exp.) | $\eta$ (V) (DFT) | PDS |
|---|---|---|---|---|
| $NaBi_5O_8$ | 0.517 | | 1.197 | $OOH^* \longrightarrow O_2{}^+H^+$ |
| $TlBiO_4$ | 0.333 | | | $OOH^* \longrightarrow O_2{}^+H^+$ |
| $Cu_4Se_3O_{10}$ | 0.520 | 0.440[33] | | $OH \longrightarrow O^{*+}H^+$ |
| $BaBiO_3$ | 0.631 | | | $OOH^* \longrightarrow O_2{}^+H^+$ |
| $Ce_2(GeO_3)_3$ | 0.546 | | | $OH \longrightarrow O^{*+}H^+$ |
| $CdSe_2O_5$ | 0.659 | | | $OH \longrightarrow O^{*+}H^+$ |
| $AgBiO_2$ | 0.548 | 0.700[22] | | $OH \longrightarrow O^{*+}H^+$ |
| $Zn(BiO_2)_2$ | 0.429 | | | $OH \longrightarrow O^{*+}H^+$ |
| $CuSeO_3$ | 0.406 | 0.440[33] | | $OH \longrightarrow O^{*+}H^+$ |
| $Cu_2SeO_4$ | 0.381 | 0.440[33] | | $H_2O^+O^* \longrightarrow OOH^{*+}H^+$ |
| $CdSeO_3$ | 0.488 | | | $OOH^* \longrightarrow O_2{}^+H^+$ |
| $FeSnO_3$ | 0.512 | | | $OH \longrightarrow O^{*+}H^+$ |
| $CoGeO_3$ | 0.496 | 0.340[34] | | $OH \longrightarrow O^{*+}H^+$ |
| $Hg_2MoO_4$ | 0.259 | | | $OH \longrightarrow O^{*+}H^+$ |
| $CdIn_2O_4$ | 0.457 | | | $H_2O^+O^* \longrightarrow OOH^{*+}H^+$ |
| $BaTl_2O_4$ | 0.544 | | | $H_2O^+O^* \longrightarrow OOH^{*+}H^+$ |
| $Cr(SbO_3)_2$ | 0.386 | | | $H_2O^+O^* \longrightarrow OOH^{*+}H^+$ |
| $Li_3BiO_4$ | 0.414 | | | $OH \longrightarrow O^{*+}H^+$ |
| $SrSe_2O_5$ | 0.254 | | | $H_2O^+O^* \longrightarrow OOH^{*+}H^+$ |
| $Ca_2Se_3O_8$ | 0.701 | | | $OOH^* \longrightarrow O_2{}^+H^+$ |
| $Cd_6(CoO_3)_5$ | 0.391 | | | $H_2O^+O^* \longrightarrow OOH^{*+}H^+$ |
| $Ag_2SeO_3$ | 0.288 | 0.192[13] | 0.806 | $H_2O^+O^* \longrightarrow OOH^{*+}H^+$ |
| $BaSe_2O_5$ | 0.661 | | | $H_2O^+O^* \longrightarrow OOH^{*+}H^+$ |
| $LuCoO_3$ | 0.559 | | | $OOH^* \longrightarrow O_2{}^+H^+$ |
| $Ag_4GeO_4$ | 0.524 | | | $OH \longrightarrow O^{*+}H^+$ |
| $CuReO_4$ | 0.332 | | | $OH \longrightarrow O^{*+}H^+$ |
| $Co_{11}CuO_{16}$ | 0.564 | 0.606[35] | | $OH \longrightarrow O^{*+}H^+$ |
| $CoSe_2O_5$ | 0.400 | | | $H_2O^+O^* \longrightarrow OOH^{*+}H^+$ |
| $Co_5SbO_8$ | 0.486 | [19] | | $OH \longrightarrow O^{*+}H^+$ |
| $NaTlO_2$ | 0.489 | | | $OH \longrightarrow O^{*+}H^+$ |
| $MgIn_2O_4$ | 0.417 | | | $H_2O^+O^* \longrightarrow OOH^{*+}H^+$ |
| $Li_7Co_5O_{12}$ | 0.381 | 0.430[14] | | $OH \longrightarrow O^{*+}H^+$ |
| $Hg_2WO_4$ | 0.679 | | | $H_2O^+O^* \longrightarrow OOH^{*+}H^+$ |
| $CuReO_4$ | 0.555 | | | $OH \longrightarrow O^{*+}H^+$ |
| $Sn_2Ge_2O_7$ | 0.552 | | | $H_2O^+O^* \longrightarrow OOH^{*+}H^+$ |
| $MnTlO_3$ | 0.196 | | 0.080 | $H_2O^+O^* \longrightarrow OOH^{*+}H^+$ |

Table 12: Overpotentials from OC22, the experimental literature, and DFT (see Figure 7(b) in the main manuscript) along with the PDS for our final set of 190 candidate (continued).

| Formula | $\eta$ (V) (OC22) | $\eta$ (V) (exp.) | $\eta$ (V) (DFT) | PDS |
|---|---|---|---|---|
| $Ag_2HgO_2$ | 0.473 | | | $OH \longrightarrow O^{*+}H^+$ |
| $Co_2NiO_4$ | 0.504 | 0.390,[36] 0.316-0.438[37] | | $OH \longrightarrow O^{*+}H^+$ |
| $Ba_8(Bi_2O_7)_3$ | 0.464 | | | $OH \longrightarrow O^{*+}H^+$ |
| $AgSbO_4$ | 0.319 | | | $OOH^* \longrightarrow O_2{}^+H^+$ |
| $MnTlO_3$ | 0.359 | | | $OH \longrightarrow O^{*+}H^+$ |
| $Ca(CoO_2)_2$ | 0.321 | 0.331[38] | | $H_2O^+O^* \longrightarrow OOH^{*+}H^+$ |
| $Tl_2SeO_4$ | 0.577 | | | $OH \longrightarrow O^{*+}H^+$ |
| $Tl_2SeO_4$ | 0.520 | | | $OH \longrightarrow O^{*+}H^+$ |
| $CaSeO_3$ | 0.603 | | | $OH \longrightarrow O^{*+}H^+$ |
| $CdCu_2O_3$ | 0.495 | | | $OH \longrightarrow O^{*+}H^+$ |
| $CuSbO_4$ | 0.364 | | | $OH \longrightarrow O^{*+}H^+$ |
| $YMn_2O_5$ | 0.540 | | | $OH \longrightarrow O^{*+}H^+$ |
| $Cu_2W_2O_7$ | 0.425 | 0.270[20] | | $OH \longrightarrow O^{*+}H^+$ |
| $Ca_3WO_6$ | 0.488 | | | $H_2O \longrightarrow OH \cdot {}^+H^+$ |
| $YCoO_3$ | 0.517 | | | $OH \longrightarrow O^{*+}H^+$ |
| $ZnCu_2O_3$ | 0.423 | 0.550[39] | | $OH \longrightarrow O^{*+}H^+$ |
| $CuNiO_2$ | 0.401 | 0.580[40] | | $H_2O^+O^* \longrightarrow OOH^{*+}H^+$ |
| $MnBiO_3$ | 0.509 | | | $OH \longrightarrow O^{*+}H^+$ |

Table 13: Overpotentials from OC22, the experimental literature, and DFT (see Figure 7(b) in the main manuscript) along with the PDS for our final set of 190 candidate (continued). All materials listed from here are unstable as bulk materials ($E_{PBX} > 0.5$ eV) but can be stabilized as nanoparticles.

| Formula | $\eta$ (V) (OC22) | $\eta$ (V) (exp.) | $\eta$ (V) (DFT) | PDS |
|---|---|---|---|---|
| $Cr_2WO_6$ | 0.252 | | | $OOH^* \longrightarrow O_2{}^+H^+$ |
| $TlCuO_2$ | 0.426 | | | $OH \longrightarrow O^{*+}H^+$ |
| $Y(FeO_2)_2$ | 0.534 | 0.214[41] | | $H_2O^+O^* \longrightarrow OOH^{*+}H^+$ |
| $Sr_2Tl_2O_5$ | 0.374 | | | $OOH^* \longrightarrow O_2{}^+H^+$ |
| $ZrCoO_3$ | 0.458 | 0.400[42] | | $OH \longrightarrow O^{*+}H^+$ |
| $TiVO_4$ | 0.584 | | | $H_2O^+O^* \longrightarrow OOH^{*+}H^+$ |
| $HfFeO_3$ | 0.529 | | | $OOH^* \longrightarrow O_2{}^+H^+$ |
| $Mn_4CuO_8$ | 0.386 | 0.150[43] | | $OH \longrightarrow O^{*+}H^+$ |
| $CoCu_2O_3$ | 0.417 | 0.606[35] | | $H_2O^+O^* \longrightarrow OOH^{*+}H^+$ |
| $MnSe_2O_5$ | 0.495 | | | $OH \longrightarrow O^{*+}H^+$ |
| $CrMoO_4$ | 0.416 | | | $OH \longrightarrow O^{*+}H^+$ |
| $KMn_2O_4$ | 0.470 | | | $H_2O^+O^* \longrightarrow OOH^{*+}H^+$ |
| $Ba_2Tl_2O_5$ | 0.336 | | | $OH \longrightarrow O^{*+}H^+$ |
| $LuMnO_3$ | 0.544 | | | $OH \longrightarrow O^{*+}H^+$ |
| $TiMnO_3$ | 0.279 | 0.400[44] | 0.559 | $OH \longrightarrow O^{*+}H^+$ |
| $KBiO_2$ | 0.267 | | 0.278 | $H_2O \longrightarrow OH \cdot {}^+H^+$ |
| $Na_5ReO_6$ | 0.298 | | 0.965 | $OH \longrightarrow O^{*+}H^+$ |
| $CuTeO_4$ | 0.537 | | | $OH \longrightarrow O^{*+}H^+$ |
| $ScCrO_3$ | 0.458 | | | $H_2O^+O^* \longrightarrow OOH^{*+}H^+$ |
| $Ta_2CrO_6$ | 0.557 | | | $OOH^* \longrightarrow O_2{}^+H^+$ |
| $MnSnO_3$ | 0.428 | | | $OH \longrightarrow O^{*+}H^+$ |
| $Li_4PbO_4$ | 0.661 | | | $H_2O \longrightarrow OH \cdot {}^+H^+$ |
| $VSbO_4$ | 0.436 | | | $OOH^* \longrightarrow O_2{}^+H^+$ |
| $ScCuO_2$ | 0.407 | | | $H_2O^+O^* \longrightarrow OOH^{*+}H^+$ |
| $Mn_2BeO_4$ | 0.324 | | | $OOH^* \longrightarrow O_2{}^+H^+$ |
| $AlCuO_2$ | 0.479 | | | $H_2O^+O^* \longrightarrow OOH^{*+}H^+$ |
| $TiCu_3O_4$ | 0.375 | | | $H_2O^+O^* \longrightarrow OOH^{*+}H^+$ |
| $Ag_2PbO_2$ | 0.434 | | | $H_2O^+O^* \longrightarrow OOH^{*+}H^+$ |
| $LuCrO_3$ | 0.435 | | | $OH \longrightarrow O^{*+}H^+$ |
| $VSeO_4$ | 0.458 | | | $OH \longrightarrow O^{*+}H^+$ |
| $Ag_3RuO_4$ | 0.601 | | | $H_2O^+O^* \longrightarrow OOH^{*+}H^+$ |
| $GePb_5O_7$ | 0.684 | | | $OH \longrightarrow O^{*+}H^+$ |
| $VCrO_4$ | 0.320 | | | $OOH^* \longrightarrow O_2{}^+H^+$ |
| $TlTeO_4$ | 0.496 | | | $H_2O \longrightarrow OH \cdot {}^+H^+$ |
| $MnSeO_3$ | 0.438 | | | $OH \longrightarrow O^{*+}H^+$ |

Table 14: Overpotentials from OC22, the experimental literature, and DFT (see Figure 7(b) in the main manuscript) along with the PDS for our final set of 190 candidate (continued).

| Formula | $\eta$ (V) (OC22) | $\eta$ (V) (exp.) | $\eta$ (V) (DFT) | PDS |
|---|---|---|---|---|
| $Li_3BiO_3$ | 0.523 | | | $OH \longrightarrow O^{*+}H^+$ |
| $VZn_2O_4$ | 0.474 | | | $H_2O^+O^* \longrightarrow OOH^{*+}H^+$ |
| $Fe_{10}O_{11}$ | 0.499 | 0.449[45] | | $H_2O^+O^* \longrightarrow OOH^{*+}H^+$ |
| $Tl_2SnO_3$ | 0.596 | | | $H_2O^+O^* \longrightarrow OOH^{*+}H^+$ |
| $ScMn_2O_4$ | 0.285 | | 0.328 | $OH \longrightarrow O^{*+}H^+$ |
| $ZrMnO_3$ | 0.501 | | | $H_2O^+O^* \longrightarrow OOH^{*+}H^+$ |
| $Li(CuO)_2$ | 0.515 | | | $OOH^* \longrightarrow O_2{}^+H^+$ |
| $Fe_{17}O_{18}$ | 0.524 | 0.449[45] | | $OH \longrightarrow O^{*+}H^+$ |
| $K_6Co_2O_7$ | 0.360 | | | $OH \longrightarrow O^{*+}H^+$ |
| $Cr_2NiO_4$ | 0.381 | 0.334[46] | | $H_2O^+O^* \longrightarrow OOH^{*+}H^+$ |
| $YCuO_2$ | 0.380 | | | $H_2O^+O^* \longrightarrow OOH^{*+}H^+$ |
| $Mn_2SnO_4$ | 0.425 | | | $OH \longrightarrow O^{*+}H^+$ |
| $MnCuO_2$ | 0.577 | 0.150[43] | | $H_2O^+O^* \longrightarrow OOH^{*+}H^+$ |
| $YCuO_2$ | 0.377 | | | $OH \longrightarrow O^{*+}H^+$ |
| $Mn_{23}FeO_{32}$ | 0.280 | 0.47[11] | 0.291 | $OH \longrightarrow O^{*+}H^+$ |
| $SrCr_2O_4$ | 0.623 | | | $H_2O^+O^* \longrightarrow OOH^{*+}H^+$ |
| $KSnO_2$ | 0.194 | | 1.314 | $OH \longrightarrow O^{*+}H^+$ |
| $CdRuO_4$ | 0.530 | 0.266[47] | | $OOH^* \longrightarrow O_2{}^+H^+$ |
| $Co(SbO_2)_2$ | 0.660 | [19] | | $OOH^* \longrightarrow O_2{}^+H^+$ |
| $Mn_2CrO_4$ | 0.371 | 0.367[48] | | $H_2O^+O^* \longrightarrow OOH^{*+}H^+$ |
| $Na_2Sb_4O_7$ | 0.355 | | | $OH \longrightarrow O^{*+}H^+$ |
| $CeCrO_3$ | 0.293 | | | $H_2O^+O^* \longrightarrow OOH^{*+}H^+$ |
| $Na_2Co_2O_3$ | 0.297 | 0.236[16] | 0.288 | $OH \longrightarrow O^{*+}H^+$ |
| $NaSb_5O_8$ | 0.517 | | | $H_2O^+O^* \longrightarrow OOH^{*+}H^+$ |
| $RuPbO_4$ | 0.640 | | | $OH \longrightarrow O^{*+}H^+$ |
| $SnRuO_4$ | 0.321 | | | $H_2O^+O^* \longrightarrow OOH^{*+}H^+$ |
| $Ti(SnO_2)_2$ | 0.476 | | | $H_2O^+O^* \longrightarrow OOH^{*+}H^+$ |
| $LiMn_3O_4$ | 0.630 | | | $OH \longrightarrow O^{*+}H^+$ |
| $K_2PbO_2$ | 0.549 | | | $OOH^* \longrightarrow O_2{}^+H^+$ |
| $Mn_2NiO_3$ | 0.470 | | | $OOH^* \longrightarrow O_2{}^+H^+$ |
| $Mn_3NiO_4$ | 0.541 | | | $H_2O^+O^* \longrightarrow OOH^{*+}H^+$ |
| $BaMn_2O_3$ | 0.624 | | | $OOH^* \longrightarrow O_2{}^+H^+$ |
| $CaMn_7O_8$ | 0.484 | 0.400-0.900[49] | | $OH \longrightarrow O^{*+}H^+$ |

# References


(1) Tran, R. et al. The Open Catalyst 2022 (OC22) Dataset and Challenges for Oxide Electrocatalysts. *ACS Catalysis* **2022**, *13*, 3066–3084.

(2) Gunasooriya, G. T. K.; Nørskov, J. K. Analysis of Acid-Stable and Active Oxides for the Oxygen Evolution Reaction. *ACS Energy Letters* **2020**, *5*, 3778–3787.

(3) Persson, K. a.; Waldwick, B.; Lazic, P.; Ceder, G. Prediction of solid-aqueous equilibria: Scheme to combine first-principles calculations of solids with experimental aqueous states. *Physical Review B - Condensed Matter and Materials Physics* **2012**, *85*, 1–12.

(4) Singh, A. K.; Zhou, L.; Shinde, A.; Suram, S. K.; Montoya, J. H.; Winston, D.; Gregoire, J. M.; Persson, K. A. Electrochemical Stability of Metastable Materials. *Chemistry of Materials* **2017**, *29*, 10159–10167.

(5) Patel, A. M.; Nørskov, J. K.; Persson, K. A.; Montoya, J. H. Efficient Pourbaix diagrams of many-element compounds. *Physical Chemistry Chemical Physics* **2019**, *21*, 25323–25327.

(6) Tran, R. Replication Data for: Rational design of oxide catalysts for OER with OC22. 2023; `https://doi.org/10.18738/T8/APJFTM`.

(7) Yu, X.; Qu, L.; Lee, C.; Peng, J.; Yan, Q.; Bai, H.; Yao, M. Bismuth-nickel bimetal nanosheets with a porous structure for efficient hydrogen production in neutral and alkaline media. *Nanoscale* **2022**, *5*.

(8) Joya, K. S.; Ahmad, Z.; Joya, Y. F.; Garcia-Esparza, A. T.; De Groot, H. J. Efficient electrochemical water oxidation in neutral and near-neutral systems with a nanoscale silver-oxide catalyst. *Nanoscale* **2016**, *8*, 15033–15040.

(9) Kuznetsov, D. A.; Peng, J.; Giordano, L.; Román-Leshkov, Y.; Shao-Horn, Y. Bismuth

Substituted Strontium Cobalt Perovskites for Catalyzing Oxygen Evolution. *Journal of Physical Chemistry C* **2020**, *124*, 6562–6570.

(10) Thorarinsdottir, A. E.; Costentin, C.; Veroneau, S. S.; Nocera, D. G. P-Block Metal Oxide Noninnocence in the Oxygen Evolution Reaction in Acid: The Case of Bismuth Oxide. *Chemistry of Materials* **2022**, *34*, 826–835.

(11) Li, M.; Xiong, Y.; Liu, X.; Bo, X.; Zhang, Y.; Han, C.; Guo, L. Facile synthesis of electrospun MFe2O4 (M = Co, Ni, Cu, Mn) spinel nanofibers with excellent electrocatalytic properties for oxygen evolution and hydrogen peroxide reduction. *Nanoscale* **2015**, *7*, 8920–8930.

(12) Si, C.; Zhang, Y.; Zhang, C.; Gao, H.; Ma, W.; Lv, L.; Zhang, Z. Mesoporous nanostructured spinel-type MFe2O4 (M = Co, Mn, Ni) oxides as efficient bi-functional electrocatalysts towards oxygen reduction and oxygen evolution. *Electrochimica Acta* **2017**, *245*, 829–838.

(13) Bibi, I.; Alrowaily, A. W.; Alyousef, H. A.; Alotaibi, B. M.; Alqurashi, H.; Dahshan, A. Reduced graphene oxide-based silver selenide nanocomposite synthesized through hydrothermal method for oxygen evolution reaction. *Journal of Alloys and Compounds* **2024**, *993*, 174626.

(14) Jiang, S.; Suo, H.; Zheng, X.; Zhang, T.; Lei, Y.; Wang, Y. X.; Lai, W. H.; Wang, G. Lightest Metal Leads to Big Change: Lithium-Mediated Metal Oxides for Oxygen Evolution Reaction. *Advanced Energy Materials* **2022**, *12*.

(15) Zan, L.; Amin, H. M.; Mostafa, E.; Abd-El-Latif, A. A.; Iqbal, S.; Baltruschat, H. Electrodeposited Cobalt Nanosheets on Smooth Silver as a Bifunctional Catalyst for OER and ORR: In Situ Structural and Catalytic Characterization. *ACS Applied Materials and Interfaces* **2022**, *14*, 55458–55470.

(16) Sun, L.; Dai, Z.; Zhong, L.; Zhao, Y.; Cheng, Y.; Chong, S.; Chen, G.; Yan, C.; Zhang, X.; Tan, H.; Zhang, L.; Dinh, K. N.; Li, S.; Ma, F.; Yan, Q. Lattice strain and atomic replacement of CoO6 octahedra in layered sodium cobalt oxide for boosted water oxidation electrocatalysis. *Applied Catalysis B: Environmental* **2021**, *297*, 120477.

(17) Arslan Hamat, B.; Aydınol, M. K. Experimental investigation on the electrocatalytic behavior of Ag-based oxides, Ag2XO4 (X= Cr, Mo, W), for the oxygen reduction reaction in alkaline media. *Journal of Solid State Chemistry* **2020**, *290*.

(18) Singh, R. N.; Koenig, J. F.; Poillerat, G.; Chartier, P. Electrochemical Studies on Protective Thin Co3 O 4 and NiCo2 O 4 Films Prepared on Titanium by Spray Pyrolysis for Oxygen Evolution. *Journal of The Electrochemical Society* **1990**, *137*, 1408–1413.

(19) Luke, S.; Chatti, M.; Yadav, A.; Kerr, B. V.; Kangsabanik, J.; Williams, T.; Cherepanov, P. V.; Johannessen, B.; Tanksale, A.; MacFarlane, D. R.; Hocking, R. K.; Alam, A.; Yella, A.; Simonov, A. N. Mixed metal-antimony oxide nanocomposites: low pH water oxidation electrocatalysts with outstanding durability at ambient and elevated temperatures. *Journal of Materials Chemistry A* **2021**, *9*, 27468–27484.

(20) Ahmed, J.; Alhokbany, N.; Ahamad, T.; Alshehri, S. M. Investigation of enhanced electro-catalytic HER/OER performances of copper tungsten oxide@reduced graphene oxide nanocomposites in alkaline and acidic media. *New J. Chem.* **2022**, *46*, 1267–1272.

(21) Arora, A.; Wadhwa, R.; Yadav, K. K.; Ankush,; Jha, M. Enhanced electrochemical oxygen generation from sillenite phase of bismuth iron oxide (Bi24Fe2O39) ultrafine particles stabilised at room temperature. *Journal of Electroanalytical Chemistry* **2024**, *958*, 118154.

(22) Simondson, D.; Chatti, M.; Gardiner, J. L.; Kerr, B. V.; Hoogeveen, D. A.; Cherepanov, P. V.; Kuschnerus, I. C.; Nguyen, T. D.; Johannessen, B.; Chang, S. L.; Macfarlane, D. R.; Hocking, R. K.; Simonov, A. N. Mixed Silver-Bismuth Oxides: A

Robust Oxygen Evolution Catalyst Operating at Low pH and Elevated Temperatures. *ACS Catalysis* **2022**, *12*, 12912–12926.

(23) Menezes, P. W.; Indra, A.; Bergmann, A.; Chernev, P.; Walter, C.; Dau, H.; Strasser, P.; Driess, M. Uncovering the prominent role of metal ions in octahedral: Versus tetrahedral sites of cobalt-zinc oxide catalysts for efficient oxidation of water. *Journal of Materials Chemistry A* **2016**, *4*, 10014–10022.

(24) Kim, T. W.; Woo, M. A.; Regis, M.; Choi, K. S. Electrochemical synthesis of spinel type ZnCo2O4 electrodes for use as oxygen evolution reaction catalysts. *Journal of Physical Chemistry Letters* **2014**, *5*, 2370–2374.

(25) Du, C.; Yang, J.; Yang, J.; Zhao, Y.; Chen, R.; Shan, B. An iron oxide -copper bismuth oxide photoelectrochemical cell for spontaneous water splitting. *International Journal of Hydrogen Energy* **2018**, *43*, 22807–22814.

(26) Balaghi, S. E.; Triana, C. A.; Patzke, G. R. Molybdenum-Doped Manganese Oxide as a Highly Efficient and Economical Water Oxidation Catalyst. *ACS Catalysis* **2020**, *10*, 2074–2087.

(27) Hausmann, J. N.; Ashton, M.; Mebs, S.; Walter, C.; Selve, S.; Haumann, M.; Sontheimer, T.; Dau, H.; Driess, M.; Menezes, P. W. Intermetallic Cobalt Indium Nanoparticles as Oxygen Evolution Reaction Precatalyst: A Non-Leaching p-Block Element. *Small* **2024**, *2309749*, 1–7.

(28) Lima, A. J.; Silva, V. D.; Raimundo, R. A.; Morales, M. A.; Simões, T. A.; Loureiro, F. J.; Fagg, D. P.; Macedo, D. A.; Nascimento, R. M. Fe-doped calcium cobaltites as electrocatalysts for oxygen evolution reaction. *Ceramics International* **2021**, *47*, 26109–26118.

(29) Hirai, S.; Yagi, S.; Seno, A.; Fujioka, M.; Ohno, T.; Matsuda, T. Enhancement of

the oxygen evolution reaction in Mn3+-based electrocatalysts: Correlation between Jahn-Teller distortion and catalytic activity. *RSC Advances* **2016**, *6*, 2019–2023.

(30) Bagheri, S.; Ramimoghadam, D.; Yousefi, A. T.; Hamid, S. B. A. Synthesis, characterization and electrocatalytic activity of silver doped-titanium dioxide nanoparticles. *International Journal of Electrochemical Science* **2015**, *10*, 3088–3097.

(31) Simondson, D.; Chatti, M.; Bonke, S. A.; Tesch, M. F.; Golnak, R.; Xiao, J.; Hoogeveen, D. A.; Cherepanov, P. V.; Gardiner, J. L.; Tricoli, A.; MacFarlane, D. R.; Simonov, A. N. Stable Acidic Water Oxidation with a Cobalt–Iron–Lead Oxide Catalyst Operating via a Cobalt-Selective Self-Healing Mechanism. *Angewandte Chemie - International Edition* **2021**, *60*, 15821–15826.

(32) Li, Y.; Zhang, X.; Zheng, Z. A Review of Transition Metal Oxygen-Evolving Catalysts Decorated by Cerium-Based Materials: Current Status and Future Prospects. *CCS Chemistry* **2022**, *4*, 31–53.

(33) Tabassum, L.; Tasnim, H.; Shubhashish, S.; Perera, I.; Bhosale, T.; Li, M.; March, S.; Islam, M. K.; Suib, S. L. Selenium-doped copper oxide nanoarrays: Robust electrocatalyst for the oxygen evolution reaction with ultralow overpotential. *Applied Materials Today* **2022**, *27*, 101485.

(34) Xu, Z.; Li, W.; Wang, X.; Wang, B.; Shi, Z.; Dong, C.; Yan, S.; Zou, Z. Novel Cobalt Germanium Hydroxide for Electrochemical Water Oxidation. *ACS Applied Materials and Interfaces* **2018**, *10*, 30357–30366.

(35) Rajput, A.; Kundu, A.; Chakraborty, B. Recent Progress on Copper-Based Electrode Materials for Overall Water-Splitting. *ChemElectroChem* **2021**, *8*, 1698–1722.

(36) Yu, M.; Budiyanto, E.; Tüysüz, H. Principles of Water Electrolysis and Recent Progress in Cobalt-, Nickel-, and Iron-Based Oxides for the Oxygen Evolution Reaction. *Angewandte Chemie - International Edition* **2022**, *61*.

(37) Cui, B.; Lin, H.; Li, J. B.; Li, X.; Yang, J.; Tao, J. Core-ring structured NiCo2O4 nanoplatelets: Synthesis, characterization, and electrocatalytic applications. *Advanced Functional Materials* **2008**, *18*, 1440–1447.

(38) Lin, X.; Bao, H.; Zheng, D.; Zhou, J.; Xiao, G.; Guan, C.; Zhang, L.; Wang, J. Q. An Efficient Family of Misfit-Layered Calcium Cobalt Oxide Catalyst for Oxygen Evolution Reaction. *Advanced Materials Interfaces* **2018**, *5*, 1–7.

(39) Yue, Y.; Niu, J.; Yang, C.; Qin, J.; Zhang, X.; Liu, R. The OER/ORR activities of copper oxyhydroxide series electrocatalysts. *Molecular Catalysis* **2023**, *537*, 112942.

(40) Wang, L.; Ge, X.; Li, Y.; Liu, J.; Huang, L.; Feng, L.; Wang, Y. Nickel enhanced the catalytic activities of amorphous copper for the oxygen evolution reaction. *Journal of Materials Chemistry A* **2017**, *5*, 4331–4334.

(41) Zhang, Q.; Liu, N.; Guan, J. Charge-Transfer Effects in Fe-Co and Fe-Co-Y Oxides for Electrocatalytic Water Oxidation Reaction. *ACS Applied Energy Materials* **2019**, *2*, 8903–8911.

(42) Huang, L.; Chen, D.; Luo, G.; Lu, Y. R.; Chen, C.; Zou, Y.; Dong, C. L.; Li, Y.; Wang, S. Zirconium-Regulation-Induced Bifunctionality in 3D Cobalt–Iron Oxide Nanosheets for Overall Water Splitting. *Advanced Materials* **2019**, *31*, 1–10.

(43) Zhou, Z.; Li, X.; Li, Q.; Zhao, Y.; Pang, H. Copper-based materials as highly active electrocatalysts for the oxygen evolution reaction. *Materials Today Chemistry* **2019**, *11*, 169–196.

(44) Frydendal, R.; Paoli, E. A.; Chorkendorff, I.; Rossmeisl, J.; Stephens, I. E. Toward an Active and Stable Catalyst for Oxygen Evolution in Acidic Media: Ti-Stabilized MnO2. *Advanced Energy Materials* **2015**, *5*.

(45) Müllner, M.; Riva, M.; Kraushofer, F.; Schmid, M.; Parkinson, G. S.; Mertens, S. F.; Diebold, U. Stability and Catalytic Performance of Reconstructed Fe 3 O 4 (001) and Fe 3 O 4 (110) Surfaces during Oxygen Evolution Reaction. *Journal of Physical Chemistry C* **2019**, *123*, 8304–8311.

(46) Babu, S. P.; Falch, A. Recent Developments on Cr-Based Electrocatalysts for the Oxygen Evolution Reaction in Alkaline Media. *ChemCatChem* **2022**, *14*, e202200364.

(47) Chen, X.; Wang, H.; Meng, R.; Xia, B.; Ma, Z. Cadmium Hydroxide: A Missing Non-Noble Metal Hydroxide Electrocatalyst for the Oxygen Evolution Reaction. *ACS Applied Energy Materials* **2020**, *3*, 1305–1310.

(48) Song, X.; Yang, T.; Du, H.; Dong, W.; Liang, Z. New binary Mn and Cr mixed oxide electrocatalysts for the oxygen evolution reaction. *Journal of Electroanalytical Chemistry* **2016**, *760*, 59–63.

(49) Han, X.; Zhang, T.; Du, J.; Cheng, F.; Chen, J. Porous calcium-manganese oxide microspheres for electrocatalytic oxygen reduction with high activity. *Chemical Science* **2013**, *4*, 368–376.